Atmos. Chem. Phys. Discuss., 13, 28751–28818, 2013
www.atmos-chem-phys-discuss.net/13/28751/2013/
doi:10.5194/acpd-13-28751-2013

Atmospheric Chemistry and Physics Discussions

The Pagami Creek smoke plume after long-range transport to the upper troposphere over Europe – aerosol properties and black carbon mixing state

F. Dahlkötter[1], M. Gysel[2], D. Sauer[1,3], A. Minikin[1], R. Baumann[1], P. Seifert[4], A. Ansmann[4], M. Fromm[5], C. Voigt[1,6], and B. Weinzierl[1,3]

[1]Deutsches Zentrum für Luft- und Raumfahrt (DLR), Institut für Physik der Atmosphäre, Oberpfaffenhofen, Germany
[2]Paul Scherrer Institute, Laboratory of Atmospheric Chemistry, Villigen, Switzerland
[3]Ludwig-Maximilians-Universität München, Meteorologisches Institut, München, Germany
[4]Leibniz-Institut für Troposphärenforschung, Leipzig, Germany
[5]Naval Research Laboratory, Washington, D.C., USA
[6]Johannes Gutenberg-Universität Mainz, Institut für Physik der Atmosphäre, Mainz, Germany

Received: 23 August 2013 – Accepted: 1 October 2013 – Published: 5 November 2013

Correspondence to: B. Weinzierl (bernadett.weinzierl@dlr.de)

Published by Copernicus Publications on behalf of the European Geosciences Union.

Abstract

During the CONCERT 2011 field experiment with the DLR research aircraft Falcon an enhanced aerosol layer with particle linear depolarization ratios of 6–8 % at 532 nm has been observed at altitudes above 10 km over northeast Germany on 16 September 2011. Dispersion simulations with HYSPLIT suggest that the elevated aerosol layer originated from the pyro-convective Pagami Creek forest fire in Minnesota, USA. The 3–4 days old smoke plume has high total refractory black carbon (rBC) mass concentrations of 0.03–0.35 $\mu g\,m^{-3}$ at standard temperature and pressure (stp) with rBC mass equivalent diameters predominantly smaller than 130 nm. Assuming a core-shell particle structure, the BC cores exhibit very thick (median: 105–136 nm) BC-free coatings, which modify the radiative transfer through this layer. A large fraction of the BC-containing particles disintegrate while passing the laser beam of the Single Particle Soot Photometer (SP2). This is shown for the first time for high-altitude aerosol layers in this study, giving evidence for heterogeneous mixing structures and possibly modified light-scattering and light-absorbing properties of the particles. This case study estimates the rBC mass import from the Pagami Creek forest fire into the upper troposphere/lower stratosphere (UTLS) region (best estimate: 25 Mg BC). A comparison to black carbon emission rates from aviation underlines the relevance of the import of forest fire aerosol on the BC load in the UTLS region. Our detailed information on the microphysics and the mixing state of the BC forest fire aerosol layer will help to better understand and investigate its radiative impact.

ACPD
13, 28751–28818, 2013

1 Introduction

Light-absorbing aerosol species, such as black carbon (BC[1]), contribute to a large part to the positive radiative forcing of aerosols (Jacobson, 2001). Recent modeling studies suggest that BC is the second strongest source, after CO_2, of global warming (Ramanathan and Carmichael, 2008) because it is the dominant solar-radiation-absorbing component in the visible spectrum in the atmosphere. A comprehensive scientific assessment of the role of BC in the climate system is given in Bond et al. (2013). In addition to BC, other light-absorbing materials such as brown carbon, a light-absorbing organic carbon (OC), can contribute significantly to light absorption (e.g. Andreae and Gelencser, 2006; Moosmüller et al., 2009). Globally, the largest source of primary carbonaceous fine particles in the global troposphere is anthropogenically and naturally occurring biomass burning[2] (Akagi et al., 2011). Thus, biomass burning has a major impact on the radiation budget of the atmosphere (Knorr et al., 2012). Diehl et al. (2012) estimate the global BC emissions from biomass burning as 1.8–7.0 $Tg\,yr^{-1}$, while OC

[1]The terminology used in the literature for the carbonaceous particles from combustion emission is often ambiguous (Petzold et al., 2013). Here we use the term "BC" exclusively for the most refractory and light-absorbing component of carbonaceous combustion particles, which is essentially pure carbon, not including organic carbon, brown carbon or inorganic aerosol components. The term "BC-containing" particle is used for referring to the whole combustion particles with some BC content. A particle is classified as a "BC-free" particle, if the Single Particle Soot Photometer (SP2) does not detect any BC in the particle, which does not exclude the presence of a small amount of BC below the lower detection limit of the SP2 ($\sim$ 0.5 fg BC in a particle). Furthermore, we use the more specific term refractory black carbon (rBC; see Petzold et al., 2013), whenever we refer to quantitative measurements of the rBC mass (or quantities inferred from rBC mass measurements) performed using the Single Particle Soot Photometer (SP2; Schwarz et al., 2006).

[2]Biomass burning is defined as the sum of all open natural and anthropogenic combustion processes using non-fossilized vegetative or organic fuels (Akagi et al., 2011). In this study, the term "biomass burning aerosol" is used if used in referenced studies. We use forest fire aerosol for the case treated in this study to separate it from the general term "biomass burning".

ACPD
13, 28751–28818, 2013

emissions range from 14–57 Tg yr^{-1}. Biomass burning emissions can be transported to the free troposphere and even the stratosphere by e.g. pyro-convection, as it was observed for a North American forest fire by Jost et al. (2004), for instance, and can form elevated aerosol layers[3]. Such light-absorbing aerosol particles in the atmosphere are often transported over long distances (e.g. Damoah et al., 2004; Mattis et al., 2008; Ramanathan and Feng, 2009) as transcontinental plumes of elevated aerosol layers (Ramanathan and Carmichael, 2008), which are observed frequently. Such long-range transport of biomass burning emissions was previously measured and reported by e.g. Fiebig et al. (2003), Petzold et al. (2007), Real et al. (2007), Tesche et al. (2009), Quennehen et al. (2011), Weinzierl et al. (2011) and Quennehen et al. (2012). Barnaba et al. (2011) estimate that up to 35 % of the aerosol optical thickness of the European fine particle fraction (< 1 µm) is attributable to wildland fire emissions, including long-range transport from North America.

During the transport, the biomass burning plumes can mix with other aerosols (e.g. Ramanathan and Carmichael, 2008; Tesche et al., 2009; Petzold et al., 2011; Weinzierl et al., 2011). Depending on the composition and altitude, these layers can have cooling or warming effects on different parts of the atmosphere. Especially BC in elevated aerosol layers absorbs incoming solar radiation effectively and transforms it into thermal radiation (Moosmüller et al., 2009). In this context, the mixing state of BC-containing particles is important as coatings with light-scattering material can enhance the absorption of the BC core due to the so-called "lensing effect" and can thus amplify the heating potential of BC-containing aerosol layers on the surrounding air (Bauer et al., 2010; Shiraiwa et al., 2010). Enhancements of the absorption by at least 30 % (Schwarz et al., 2008b) up to 100 % have been found for thickly coated particles with a ratio of the optical particle diameter to the core diameter (D_{opt}/D_{rBC}) of 2 (Shiraiwa et al., 2010). However, Cappa et al. (2012) report a significant difference in the absorption enhancement by coatings between ambient observations and model results. Thus,

[3]In this study, we define an elevated aerosol layer as a vertically extended layer, containing aerosol particles situated above the planetary boundary layer.

ACPD
13, 28751–28818, 2013

the understanding of the absorption enhancement and the radiative forcing by mixed atmospheric BC is still incomplete and needs further investigations. Aside from this idealized internal shell-core mixture of particles, more complex structures of BC particles and BC-free materials exist in nature (e.g. Sedlacek et al., 2012). Semi-external mixtures such as particles attached to each other or near-surface BC cores can be observed in the atmosphere as well (Mishchenko et al., 2004; Liu and Mishchenko, 2007). Nevertheless, most modeling studies assume homogeneously mixed or idealized core-shell morphologies as a basis for radiative transfer calculations though recent model developments implement the particle mixing state (e.g. Aquila et al., 2011). More information about particle mixing is given in Buseck and Posfai (1999), Posfai et al. (2003), and Posfai et al. (2004). Additionally, the structure of mixed particles, e.g. internal mixing of a BC core with organic or inorganic aerosol components, might have an influence on the activation of BC particles to form cloud droplets in warmer regimes, possibly leading to BC wet deposition and a related decrease in BC residence times, and on the ice nucleation efficiency of the particle and is thus relevant for the indirect climate effect of aerosols (Hoose and Möhler, 2012).

However, many processes are not yet investigated in detail and elevated light-absorbing aerosol layers and their impact on the radiation budget are only insufficiently quantified and characterized. One reason for this deficiency is the sparseness of airborne in-situ measurements in elevated aerosol layers. However, recently more studies focus on the distribution of BC in the troposphere, for instance in elevated aerosol layers with enhanced BC concentrations, assessed by airborne measurements (e.g. McMeeking et al., 2010; Schwarz et al., 2010). The findings based on measured optical and microphysical properties of these elevated aerosol layers can improve the quantification of their impact on the radiation budget and on aviation. The latter can be relevant e.g. in the case of volcanic ash layers, which can pose a hazard for aircraft turbines.

This study addresses the airborne in-situ characterization and quantification of aerosol particles in an elevated forest fire aerosol layer observed on 16 Septem-

ACPD
13, 28751–28818, 2013

ber 2011 over northeast Germany, originating from the Pagami Creek forest fire plume after long range transport. We present data collected with the DLR research aircraft Falcon-20E in the framework of the CONtrail and Cirrus ExpeRimenT 2011 (CONCERT 2011) in September 2011 in Central Europe.

2 Material and methods

2.1 Research flights and instrumentation

Within the framework of CONCERT two aircraft field experiments were performed. The major scope of the CONCERT missions in 2008 and 2011 (Voigt et al., 2010) is to measure microphysical and optical properties of contrail cirrus (Voigt et al., 2011; Schumann et al., 2011) and natural cirrus in order to investigate their climate impact (Kübbeler et al., 2011; Schumann et al., 2013; Jeßberger et al., 2013). In addition, volcanic aerosol layers from the stratospheric eruption of the Kasatochi in 2008 (Jurkat et al., 2010; Schmale et al., 2010) and the quiescently degassing Etna in 2011 have been probed. Here we focus on the observation of an enhanced aerosol layer in the upper troposphere/lower stratosphere (UTLS) region, originating from a forest fire. During CONCERT 2011, the DLR Falcon research aircraft was based in Oberpfaffenhofen (Germany) and performed 11 research flights between 7 September and 30 September 2011. Most of the flights were conducted over Germany, with additional landings in Norway and Italy. Instruments from DLR and the Universities of Mainz and Clermont-Ferrand were operated onboard the DLR Falcon. The following basic aerosol parameters where measured: particle size distribution, rBC mass concentration, rBC core size distribution, mixing state of rBC-free and rBC-containing particles, light scattering coefficient and light absorption coefficient. In addition, instruments for trace gases such as CH_4, CO_2, H_2O, HCl, HNO_3, HONO, NO, NO_y, O_3 and SO_2 were deployed on the Falcon. In the following, we only describe the instruments used in this study.

ACPD
13, 28751–28818, 2013

In the past decades BC measurements in the atmosphere were conducted predominantly with filter-based instruments. In this study, the more recently introduced Single Particle Soot Photometer (SP2; Stephens et al., 2003) was applied to obtain information about the rBC mass concentration as well as the mixing state and coating thickness of rBC-containing particles. The SP2 determines the optical size and the rBC mass of single rBC-containing particles, using light-scattering and laser-induced incandescence methods, respectively (Schwarz et al., 2006). More details about the functional principles, calibration and data analysis approaches of the SP2 will be summarized in Sect. 2.2.

To obtain information on the entire aerosol size distribution, measurements from five condensation particle counters (CPC/CPSA) set to different (4 nm, 10 nm, 14 nm) lower cut-off diameters are combined with optical sizing measurements from the SP2 and a wing-mounted instrument of type Forward Scattering Spectrometer Probe (FSSP-300). Table 1 summarizes the aerosol parameters and the size ranges covered by the different aerosol in-situ instruments used in this study.

2.2 Instrument calibration and data analysis

In the SP2, a concentric-nozzle jet system is used to direct the aerosol sample flow through a high-intensity continuous-wave intra-cavity laser beam (λ = 1064 nm) and four different detectors are used to characterize individual particles with 100 % detection efficiency within the respective detection limits (see Table 1). The response curves of four detectors for each particle are recorded for 44 µs with a temporal resolution of 0.2 µs.

In our instrument the standard Droplet Measurement Technologies Inc. (DMT) broadband incandescence detector (BID) and the standard DMT narrowband incandescence detector (NID) are used to detect the thermal radiation emitted by light-absorbing and refractory particles heated to incandescence in the wavelengths bands 300–800 nm and 630–800 nm, respectively. The peak intensity of the thermal radiation is typically reached at the vaporization temperature of the most refractory particle component.

ACPD
13, 28751–28818, 2013

The incandescence signals from atmospheric aerosol particles normally originate from rBC and the peak height is proportional to the rBC mass in a particle, independent of particle morphology or coatings with non-refractory aerosols components (Schwarz et al., 2006; Moteki and Kondo, 2007, 2010). The BID and NID are empirically calibrated using the fullerene soot batch from Alfa Aesar (stock #40971, lot #FS12S011), which has been shown to provide equal incandescence detector response per mass as atmospheric rBC (Moteki and Kondo, 2010; Laborde et al., 2012a), and which is recommended as the most suitable SP2 calibration material for atmospheric rBC applications (Baumgardner et al., 2012). The mass equivalent diameter of the rBC cores, D_{rBC}, is calculated from the measured rBC mass, assuming void-free spherical rBC cores and an rBC material density of 1800 kg m^{-3}. The applied design of the SP2 and the gain settings used for the CONCERT 2011 field experiment limits rBC core measurements and the rBC mass size distribution to a range of approximately $80 < D_{rBC} < 440$ nm ($0.5 < m_{rBC} < 80.3$ fg; see also Table 1). The contribution of BC cores outside the detection range of the SP2 to the integral total rBC mass concentration was accounted for by extrapolating the measured rBC mass size distribution with a log-normal fit (see schematic in Fig. 1). For the CONCERT 2011 data set, the log-normal distribution was fitted to the measured rBC core mass size distribution in the range between 80–250 nm (the size range between 250 nm and the upper detection limit was not considered for fitting in order to avoid fitting biases from insufficient counting statistics in this range). This approach provides reliable results as the mass size distributions, generally of log-normal shape in good approximation, have the peak (i.e. the mass median diameter; MMD) in the fitted size range. In our case, this extrapolation accounts for 20 % of the total rBC mass.

A light scattering detector (LSD) detects elastically scattered light at 1064 nm wavelength. The LSD signal is used for the optical sizing of the particles. rBC-free particles, i.e. non-absorbing particles, assuming rBC being the main light-absorbing component, cross the laser beam unaltered and the peak amplitude of the LSD signal is proportional to the scattering cross-section of the particle. Certified polystyrene Latex (PSL;

ACPD
13, 28751–28818, 2013

refractive index = 1.59) size standards are used to calibrate the scattering cross-section measurement of the LSD detector as described in Laborde et al. (2012b). The optical size of rBC-free particles is inferred from the measured scattering cross-section, using Mie theory for a homogeneous sphere and assuming a refractive index of 1.59 (see below). For the SP2 settings used here, the LSD covers a size range of the optical diameters of roughly 140–290 nm (Table 1).

Particles containing rBC heat up as they pass the laser beam, thereby resulting in evaporation of the rBC-free coatings and eventually even the rBC core. Therefore the peak amplitude of the LSD signal does not represent the scattering cross-section of the undisturbed particles. However, Gao et al. (2007) introduced the position sensitive detector (PSD), a modified multi-element LSD, which makes it possible to determine the scattering cross-section of rBC-free as well as rBC-containing particles at any time (position) in the laser beam. The approach for the time-resolved scattering cross-section analysis applied here, described in detail elsewhere (Laborde et al., 2012a), is largely based on Gao's method, but using the actual laser beam profile rather than assuming a perfect Gaussian beam shape. The scattering cross-section of the unperturbed particle is obtained from the LSD signal in the leading edge of the laser beam (up to 3 % of maximal laser intensity) before the onset of coating evaporation. This is commonly referred to as the leading-edge-only (LEO) fit method (Gao et al., 2007). The LEO-fit extends the upper detection limit for the optical sizing of rBC-free particles to larger diameters, in our case up to around 550 nm (Table 1). Similar to the standard optical sizing (see above), the optical diameter of rBC-free particles is inferred from the scattering cross-section measured with the LEO-fit approach assuming a homogeneous sphere and a refractive index of 1.59 + 0.00i (see below). Inferring the optical size of rBC-containing particles from their scattering cross-section is not straight forward as the particles are inhomogeneous and typically not spherical. We use the approach described in Schwarz et al. (2008b) and Laborde et al. (2012b). Briefly, a concentric-spheres core-shell morphology is assumed for the Mie calculations. The core size is constrained by the rBC core mass equivalent diameter, D_{rBC}, from the incandescence

ACPD
13, 28751–28818, 2013

measurement. To obtain the total optical diameter, D_{opt}, of the unperturbed particle, including core and shell, the diameter of the total particle is varied until the calculated scattering cross-section matches the measured scattering cross-section. The coating thickness (Δ_{coat}) of a BC-containing particle is defined as the difference between the radii of the unperturbed particle and the BC core, i.e. $\Delta_{coat} = 0.5\,(D_{opt}–D_{rBC})$. This provides information about the mixing state of individual BC-containing particles. In this study, refractive indices of 2.26–1.26i and 1.59–0.00i are used for the rBC core and the coating, respectively, in the Mie calculations. The particular value for the refractive index of the BC core was measured by Moteki et al. (2010) for thermally denuded ambient BC particles using an APM (Aerosol Particle Mass Analyzer) and an SP2.

The reliability of the SP2 has been studied extensively by inter-comparisons of six different SP2s at the AIDA chamber in November 2011. Laborde et al. (2012b) report a reproducibility of 10 % for the rBC mass and 17 % for the coating thicknesses for this inter-comparison study. However, due to calibration uncertainties the absolute uncertainty may be higher. Kondo et al. (2011b) compared rBC mass concentrations measured with the SP2 and a filter-based absorption photometer continuous soot monitoring system (COSMOS) and found that the methods agree to within about 10 % on average. Besides, Laborde et al. (2013) made a comparison of the rBC measurements by the SP2 with a collocated EC measurement by a thermal-optical EC instrument (Sunset ECOC analyzer), revealing agreement well within the uncertainty of either method. The SP2 was prepared for the research flights, following the instructions given in Laborde et al. (2012b). For this study we assume an uncertainty of 15 % for the rBC mass, which includes the described reproducibility, calibration uncertainties and uncertainties due to airborne in-situ measurements.

To obtain particle number size distributions of the whole aerosol, measurements from the SP2 and the FSSP-300 are combined. To ensure a correct signal-to-diameter assignment for the optical particle counters such as the FSSP-300 ($\lambda = 633$ nm), an appropriate refractive index has to be applied for the bulk aerosol. Problems with this procedure are explained in more detail in e.g. Weinzierl et al. (2009). Real parts of

ACPD
13, 28751–28818, 2013

the refractive index at visible wavelengths of several types of organic aerosols and biomass burning organic aerosol are reported to be 1.50–1.63 and about 1.56–1.64, respectively (Kondo et al., 2011a, and references therein). However, the FSSP-300 cannot distinguish between BC-free and BC-containing particles. Thus, the particles in the considered FSSP-300 size range are assumed to be non-absorbing (zero imaginary part of the complex refractive index), with real parts of the bulk refractive index of 1.59–1.60. That increases the uncertainty of the FSSP-300 data compared to the SP2 size distribution, which distinguishes between BC-containing and BC-free particles. However, due to a low fraction of BC-containing particles in the data set presented later (8–13 %) we expect only minor effects of the refractive index assumption on the particle size distribution. The combination of the FSSP-300 and the SP2 data allows us to derive the particle number size distribution in the size range between about 0.14 µm and 30 µm (Table 1). To obtain information on the size distribution in the Aitken mode (D_{opt} < 0.14 µm) data from the CPC/CPSA is added. The number concentration of Aitken mode particles in the size range between 0.01 µm (lower CPC cut-off) and 0.14 µm (lower SP2 cut-off) is determined as the differential of particles in the accumulation mode, i.e. measured with the SP2 and the FSSP-300 and the integral number concentration determined by the CPC/CPSA. This method is only valid if nucleation mode particles can be excluded. This is ensured by the measurement of particles in the size range 4–10 nm, showing low particle number concentrations. The shape of the particle number size distribution in the Aitken mode range is approximated by applying a log-normal fit, assuming that a single log-normal mode represents all particles in the Aitken mode (Weinzierl et al., 2011) with the particular minimum between Aitken and accumulation mode being operationally defined as 0.14 µm. Figure 2 sketches the procedure for fitting the number size distributions. The parameters for a log-normal fit of mode j are the mode number concentration (N_j), the geometric standard deviation (GSD_j), and the count median diameter (CMD_j). The CMD for the Aitken mode, CMD_1, is set constant to 0.07 µm, and GSD_1 is estimated to provide the best fit to the residual between the measured accumulation mode and the lognormal fit to the accumulation

ACPD
13, 28751–28818, 2013

mode in the lower end of the measurement range (of SP2/FSSP-300) and to match values regularly found for forest fire aerosol layers (see Sect. 5.3). In addition to one log-normal distribution used to describe the size distribution in the Aitken mode, one or two log-normal distributions are applied to parameterize the particle size distribution in the accumulation mode and the coarse mode, i.e. the measured size range of the SP2 and FSSP-300. Because no considerable fraction of particles was measured in the coarse mode, in the following we spare to mention this mode.

Unless stated otherwise, the data presented in this study refer to standard temperature and pressure (stp; 273.15 K, 1013.25 hPa), corresponding to mixing ratios. stp concentration data can be converted to ambient conditions by applying a factor f_{stp} indicated in Table 3.

To determine the origin and the dispersion of the investigated aerosol, we use the Hybrid Single Particle Lagrangian Integrated Trajectory Model HYSPLIT (Draxler and Hess, 1997, 1998). Input for the dispersion calculations is the location of the forest fire and the altitude range of the emission. For the HYSPLIT dispersion runs the following assumptions are made: the dispersion is calculated for 0.5° grid cells for 3 h time steps. All particles are set to a diameter of 1 µm and a particle density of 1 g cm^{-3}. The particle deposition velocity is assumed to be 0.1 mm s^{-1} for all particles. Wet deposition is not considered for this qualitative approach. HYSPLIT is initialized with meteorological data from the European Centre for Medium-Range Weather Forecasts (ECMWF) and the Global Forecast System (GFS). In this study only the results for the ECMWF data are presented because no relevant differences are observed for the different meteorological data sets.

ACPD
13, 28751–28818, 2013

3 Results: the 16 September 2011 case with respect to the average situation

3.1 Aerosol layers and vertical aerosol distribution during CONCERT 2011

Although the localization and observation of elevated aerosol layers was not a scientific objective of CONCERT 2011, in 9 of the 11 flights elevated aerosol layers were observed. From about 32.3 h total flight time we flew by chance roughly 3.2 h (~10 % of the flight time) within elevated aerosol layers (volcanic ash layers, which we intentionally measured, are not counted here). Table 2 gives an overview of all CONCERT 2011 flights, including the altitude of the detected aerosol layers. As can be seen from Table 2, most of the aerosol layers were found between 2 km and 5 km altitude. Figure 3 shows the median vertical profile of the rBC mass concentration and the rBC mass mixing ratio for the entire CONCERT 2011 field experiment, i.e. for all 11 research flights, with 500 m vertical resolution and a temporal resolution of 10 s. This temporal resolution is used on the one hand to exclude noise from insufficient integration time and on the other hand to retain the horizontal resolution, which is about 2 km at a temporal resolution of 10 s. The rBC mass mixing ratio (MMR) is calculated from the mass concentration m at standard conditions and the density of dry air at standard conditions ($\rho_0 = 1.29\,\mathrm{kg\,m^{-3}}$): MMR [$\mathrm{ng\,kg^{-1}}$] = m_{stp} [$\mathrm{ng\,m^{-3}}$]/ρ_0 [$\mathrm{kg\,m^{-3}}$]. The median vertical distribution can be used as an approximation of the typical vertical profile of BC above Central Europe during autumn 2011. Below roughly 2 km altitude the vertical profile is dominated by the influence of the boundary layer: we see the highest MMR, a small spread between 10-/90-percentiles and a decreasing rBC MMR with increasing altitude. Above 2 km the signal is dominated by the wide spread of the percentile values, showing a high variability in rBC mixing ratios above the boundary layer. This variability can be attributed to the presence of aerosol layers as a source of heterogeneous aerosol loadings in the free troposphere. The highest variability is found above 10 km altitude. The strongly increased 75- and 90-percentile values at this altitude are related to the high loadings detected in an aerosol layer that was crossed in the UTLS region between 10 km and 12 km during the two flights on 16 September 2011. We will

ACPD
13, 28751–28818, 2013

show in Sect. 4 that this aerosol layer is part of the Pagami Creek forest fire smoke plume after ~ 4 days of long-range transport from North America to Europe, but in the following we will first focus on the aerosol properties in this forest fire plume in detail.

3.2 Vertical dimension of the forest fire aerosol layer

On 16 September 2011, two flights were performed with the DLR Falcon. For the first flight (#110916a, 10:48–13:20 UTC), the Falcon flew from Oberpfaffenhofen (EDMO; 48°05′ N, 11°16′ E, 593 m a.s.l.) to Neubrandenburg-Trollenhagen (ETNU; 53°36′ N, 13°18′ E, 69 m a.s.l.), both in Germany. The second flight (#110916b, 14:54–17:48 UTC) was from Neubrandenburg-Trollenhagen back to Oberpfaffenhofen. The scope of these two flights was to sample contrails from commercial aircraft. To achieve this, the aircraft climbed up to more than 10 km altitude and stayed at altitudes between 10.0 km and 11.8 km for roughly 105 min and 95 min during the flights #110916a and #110916b, respectively. In the following analysis, we exclude encounters from aircraft emissions and contrails from the observations of the extended aerosol layer, using NO_y or SO_2 as aircraft plume markers. We explicitly investigate the chemical, microphysical and optical properties of the forest fire plume aerosol. Figure 4 shows the time series of rBC mass concentration for both flights. The elevated rBC mass concentrations at high altitudes (> 10 km a.s.l.) of the Pagami Creek forest fire plume[4], already identified in the vertical profiles presented in Sect. 3.1 and Fig. 3, are clearly seen in Fig. 4. The Pagami Creek forest fire plume was also visible by eye as distinct broad greyish-brownish aerosol layer (Fig. 5). Figure 6 gives an overview of the horizontal distribution of the forest fire aerosol layer during the two flights on 16 September 2011 by means of color-coded rBC mass concentrations (size range: 80–440 nm) along the flight track. To emphasize upper tropospheric BC, we show only values for rBC mass concentrations

[4]In this study we refer to the observed aerosol layer observed over Germany as Pagami Creek fire aerosol layer or Pagami Creek fire plume, being aware of that the observed layer does not contain the entire emissions of the Pagami Creek fire and smaller layers and plumes were transported along other trajectories at other altitudes.

ACPD
13, 28751–28818, 2013

above 9 km a.s.l. Observed rBC mass concentrations were as high as 0.67 $\mu g\,m^{-3}$ (stp) and covered a large area over northeastern Germany. For comparison, maximum rBC mass concentrations in the polluted boundary layer over Munich, averaged for 10 s, showed similar values with roughly 0.70 $\mu g\,m^{-3}$ on that day.

Figure 7 shows vertical profiles of number concentrations of rBC-free and rBC-containing particles, and rBC mass concentration for both flights with 100 m vertical resolution, including the median and 10-/25-/75-/90-percentiles for the specific size ranges 140–290 nm (rBC-free particles) and 80–440 nm (rBC-containing particles). The vertical profiles are averaged over the entire flight for altitudes > 2 km. For altitudes < 2 km the profiles are separately shown for the planetary boundary layer (PBL) over Oberpfaffenhofen and Neubrandenburg-Trollenhagen. A prominent feature in both vertical profiles is the presence of increased aerosol concentrations at altitudes above 10 km a.s.l. These signals above 10 km (Fig. 7) show a distinct difference to the median value of Fig. 3, which represents the typical situation in September above Central Europe, and dominate the 75- and 90-percentile in Fig. 3. According to Fig. 7, the Falcon did not reach the top of the aerosol layer. However, not only the Falcon but also the ground-based lidar at Leipzig observed this aerosol layer on 16 September 2011 in the UTLS. Figure 8 presents lidar observations performed at Leipzig, Germany (51.3° N, 12.4° E), between 08:36 UTC and 10:30 UTC on 16 September 2011. In the time series of the 532 nm range-corrected backscatter signal (Fig. 8a), enhanced aerosol concentrations were observed at altitudes between 8 km and 12 km a.s.l. A humid layer was present below 1.5 km altitude, which causes the vertically striped pattern in the signal of the forest fire plume in the UTLS due to partial attenuation of the laser light by thin clouds or haze. The base of the aerosol plume slowly descended with time. In the course of the late morning around 10:30 UTC the layer diminished. The time resolved lidar profiles strongly confirm our observations, showing the maximum of the forest fire layer between 10.0 km and 11.5 km a.s.l. and an upper limit of the plume at roughly 12 km. In addition, a heterogeneously layered structure of the plume is discernible. At the time of the Falcon flyover (15:43 UTC), neither the DLR Falcon nor the

ACPD
13, 28751–28818, 2013

lidar observed signatures of the aerosol layer. In agreement to the lidar and in-situ observations, CALIPSO (not shown[5]) observed the aerosol layer on 16 September 2011 in about 10–12 km altitude in Europe.

3.3 Microphysical properties of the observed aerosol layer

To derive particle number size distributions and BC mass distributions and to infer BC particle mixing state, we subdivide the measurements in the forest fire layer into sequences with rather homogeneous rBC mass concentrations. Altogether, 14 time sequences are chosen as shown in Fig. 4. The 14 sequences include sequences with maximum concentrations as well as less concentrated sequences within this heterogeneous aerosol layer, excluding aircraft exhaust sequences, which are characterized by short and distinct increases of particle and trace gas concentrations.

3.3.1 rBC mass size distributions

Figure 9 shows the rBC mass size distribution of the forest fire plume. Plotted are the maximum and the minimum measured rBC mass size distribution. Error bars represent 15 % uncertainties. The total rBC mass concentration was estimated with adding the extrapolated tails (log-normal fit to the measurement) of the rBC mass size distribution to the rBC measurement of the SP2 integrated over the whole detection range (see Sect. 2.2 for details). The size distribution tails consistently contributed ~ 20 % to the total estimated rBC mass for each of the 14 forest fire plume sequences. Due to a higher fraction of fresh and small rBC-particles, in the boundary layer the measured rBC mass fraction might be lower, possibly implying a systematic uncertainty for the comparison of the measured rBC mass of the forest fire plume and the boundary layer (Sect. 3.2). The mass median diameter (MMD), which is equal to the modal diameter for a log-normal size distribution, of all mass size distributions of the Pagami Creek fire

[5] http://www-calipso.larc.nasa.gov/products/lidar/browse_ images/show_ date.php?s=production& v=V3-01& browse_ date=2011-09-16

ACPD
13, 28751–28818, 2013

plume is in the size range between 120 nm and 160 nm. The total rBC mass concentrations for the 14 sequences (0.03–0.35 µg m^{-3}; stp) reveal a variability of almost a factor of 10. A UTLS background sequence at the same altitude as the Pagami Creek fire plume shows rBC average total mass concentrations < 0.01 µg m^{-3} (stp), implying the Pagami Creek fire plume contains a factor of 3–34 higher rBC mass concentrations than the background. Parameters of the log-normal fit to the rBC mass size distribution (stp) and the total rBC mass concentrations derived from the log-normal fit (stp) are shown in Table 3.

3.3.2 Total particle number size distributions

Figure 10 shows the total particle number size distributions of the forest fire plume in comparison with a background aerosol sequence. The presented minimum, median, and maximum size distributions represent the range of observations for the 14 considered sequences (Fig. 4) in the forest fire aerosol layer. The parameters of the fitted total number size distributions (Fig. 10) are shown in Table 3. Additionally, factors to convert the data from stp to ambient conditions are given. For the Aitken mode (j = 1), i.e. particles < 0.14 µm (Table 3), the number concentration (N_1) is directly inferred from the measurements (see Sect. 2.2), while CMD_1 has to be assumed and GSD_1 is iteratively approximated. The minimum and the maximum values of N_1 for all 14 sequences are 760 cm^{-3} and 2228 cm^{-3}, respectively. The total number concentrations in the measured size range (accumulation mode) vary roughly by a factor of 7 within the 14 sequences as an indication of a heterogeneous distribution within the vertical column. In the accumulation mode the total number concentrations are factors of 14–100 times higher compared to the UTLS background sequence.

3.3.3 Optical properties

To assess the vertical distribution of the aerosol layer, ground-based lidar measurements are used. The vertical profiles of particle backscatter coefficient β_{par} and par-

ACPD
13, 28751–28818, 2013

ticle linear depolarization ratio δ_{par} are presented in Fig. 8b based on the averaged 532 nm elastic backscatter signal of the time period from 08:36–09:25 UTC. Sequences strongly affected by the low-level clouds are removed from the analysis to increase the signal-to-noise ratio. Because no Raman-scattering information is available, the lidar data analysis is performed using the Klett–Fernald-method (Klett, 1981; Fernald, 1984). This requires the assumption of the extinction-to-backscatter ratio (lidar ratio). Because earlier studies (Tesche et al., 2011; Groß et al., 2013) show that a lidar ratio of 70 sr is reasonable for biomass burning aerosol, we use this value for the analysis of the lidar data. Uncertainties in the retrieved optical properties are due to noise and the assumption of a reference value for the lidar ratio (Rocadenbosch et al., 2010). Particle linear depolarization ratios of around 6–8 % at 532 nm are observed throughout the layer between 8 km and 12 km altitude.

4 Identification of the Pagami Creek forest fire as the source of the observed aerosol layer

Figure 11a shows a true-color image of the Pagami Creek fire located in Minnesota, USA (approximate location 47°52′ N, 91°30′ W; US Forest Service), taken by the Moderate Resolution Imaging Spectroradiometer (MODIS) on 12 September 2011 at 18:50 UTC. This fire was caused by lightning on 18 August 2011. Before 12 September the fire did not evolve significantly and thus caused only minor pollution according to the MODIS images. On 12 September 2011 the fire grew rapidly exhibiting a thick plume, which is transported eastwards (Fig. 11a). The Pagami Creek fire burned a total area of roughly 375 km^2. A cloud-top 11.0 µm brightness temperature of roughly −60 °C, corresponding to altitudes > 11 km, was observed with MODIS, which is comparable to deep thunderstorm clouds and is indeed colder than at any level up to 16 km in the radiosonde observation (RAOB) at International Falls, Minnesota, that day. Thus, this brightness temperature minimum certainly indicates cloud top altitudes up to the cold point above 12 km altitude. Radar echotops on the cloud anvil reach ∼ 13.6 km

ACPD
13, 28751–28818, 2013

at 19:54 UTC caused by pyro-convection forming this pyrocumulonimbus (PyroCb) cloud as a result of the extensive forest fire (Fromm et al., 2010). Similar observations of brightness temperatures for pyro-convective clouds are discussed in Damoah et al. (2006). Further pyro-convection events are observed and described in Andreae et al. (2004) and Fromm et al. (2005). MODIS imagery suggests that the bulk emission and the pyro-convection event were limited from roughly 17:00 UTC on 12 September to 04:15 UTC on 13 September. In fact, AVHRR imagery (not shown) suggests that pyro-convective lofting shut down at sometime between 20:41 UTC and 22:41 UTC on 12 September.

To evaluate whether the aerosol plumes observed by the Falcon over Germany on 16 September originated from the Pagami Creek fire, we conduct HYSPLIT dispersion calculations starting at the location of the Pagami Creek fire. Based on the described observations, we assume that the Pagami Creek fire released emissions for 12 h between 17:00 UTC on 12 September 2011 and 05:00 UTC on 13 September 2011 as a maximum estimate. The release location is retrieved from satellite images and the release altitude is set from ground to 11 km a.g.l., assuming pyro-convention (e.g. Fromm et al., 2005; Damoah et al., 2006) and a homogeneous vertical distribution. Results are presented in Fig. 11b–f, which show the column-integrated (6–14 km a.s.l.) particle number concentration (arbitrary units; a.u.) in the time from 20:00–23:00 UTC between 12 September and 16 September 2011. The calculations underline that the Pagami Creek fire plume was transported through the area and at the altitude where the aerosol layer has been measured by the Falcon and the lidar in Leipzig. According to those simulations the Pagami Creek plume should have reached Germany on 15 September 2011 (Fig. 11e). A detailed analysis of the simulation results suggests that the smoke layer was north of Leipzig on 15 September, explaining why the lidar in Leipzig did not detect the Pagami Creek plume on that day. Figure 11g–h show zoomed-in dispersion calculations of column-integrated (10–12 km a.s.l.) particle number concentrations on 16 September 2011 for Central Europe for the time between 08:00–11:00 UTC (g), 11:00–14:00 UTC (h) and 14–17 UTC (i). Figure 11h and i ad-

ACPD
13, 28751–28818, 2013

ditionally include the Falcon flight tracks of flight #110916a (10:48–13:20 UTC) and #110916b (14:54–17:48 UTC), respectively. Comparing the location of the measured plume and the plume location simulated by the dispersion calculations strongly suggest that the Pagami Creek fire is most likely the source of the observed aerosol layer. This is also supported by observations of CO, a tracer for biomass burning, by the Infrared Atmospheric Sounding Interferometer (IASI), showing the same transportation pattern of the plume as the dispersion calculations. According to the simulations shown in Fig. 11g–i, it seems that the measurements with the Falcon were conducted in the tail of the plume when the maximum had already passed Germany, although for the plume position an uncertainty of 5–20 % needs to be assumed. However, the simulation is also in agreement with the lidar measurements, which show that the forest fire aerosol layer was no longer observed later than 10:30 UTC (Fig. 8). Thus, only the edges of the Pagami Creek plume passed over the Leipzig lidar system. Summarizing, the presented findings show that the dispersion calculations fit well to the measurements, supporting the hypothesis that the pyro-convective Pagami Creek fire is the source of the observed aerosol layer.

5 Discussion

5.1 Estimates on the dimension and classification of the observed Pagami Creek fire plume

Under the assumption that the aerosol layer was located at DLR Falcon cruise altitude, i.e. between 10 km and 12 km, we can conclude from Figs. 4 and 6 that the aerosol layer was limited southward roughly to 52° N. That is supported by the lidar measurements in Leipzig, which detected the layer only until 10:00 UTC. It is not possible to determine the northern boundary of the layer because the Falcon flight track did not reach far enough north so that we still observed the layer at the northernmost location of the flights (∼ 54° N), indicating that the aerosol layer had a horizontal extent of at least

ACPD
13, 28751–28818, 2013

200 km. The observed and simulated distribution of the plume is supported by data of the GOME-2 Absorbing Aerosol Index (not shown; http://www.temis.nl) (de Graaf et al., 2005), showing the overall distribution of the plume.

For the size ranges 80–440 nm (rBC-containing particles) and 140–290 nm (rBC-free particles) in the accumulation mode, in the Pagami Creek forest fire plume the rBC-containing particle number concentrations of up to 300 cm^{-3} (stp) and rBC-free particle number concentrations up to 1300 cm^{-3} (stp) (Fig. 7) are more than a factor 10 larger compared to the background concentration at that altitude. In addition, the concentrations in the plume are comparable to the concentrations of the polluted boundary layer (rBC-containing particle number concentrations: up to 600 cm^{-3}; rBC-free particle number concentrations: up to 600 cm^{-3}; stp) in the respective size ranges (see above), illustrating the unexpectedly high particle number concentrations of the Pagami Creek fire plume in the UTLS region. The rBC-free particle number concentration is consistently higher than in the polluted PBL and the rBC number concentration is higher than the cleaner PBL of Neubrandenburg and all other observed aerosol layers on that day but not quite as high as in the area of Oberpfaffenhofen and Munich.

Particle linear depolarization ratios derived by the lidar observations of around 6–8 % are comparable to findings by Groß et al. (2013) who presented particle linear depolarization ratios of 7 ± 2 % for aged biomass burning aerosol from their own measurements and summarized that values between 2 % and 8 % are reported in the literature for aged biomass burning aerosol. Müller et al. (2007) report that particle linear depolarization ratios < 5 % can be expected for biomass burning aerosol particles, probably due to their spherical shape. However, in agreement with our results, Müller et al. (2007) observed during LACE 98 particle linear depolarization ratios of up to 10 % at 532 nm wavelength, which they explained by soil dust particles possibly lifted together with the smoke particles at the source of the fire. Weinzierl et al. (2011) report particle linear depolarization ratios of 6–16 % (median: 13 %) at 532 nm wavelength for biomass burning aerosol mixed with mineral dust from the Sahara measured during the SAMUM-2 field experiment in the Cape Verde region. Other aerosol types can be excluded as source of

ACPD
13, 28751–28818, 2013

the observed layer with ice clouds and mineral dust having higher and sea salt and sulphates having lower particle linear depolarization ratios (Groß et al., 2013). A mixture of ash and sulphate of volcanic origin could also explain the observed depolarization ratios besides biomass burning aerosol. However, volcanic eruptions did not occur in an appropriate spatio-temporal window. In addition normally no enhanced BC is observed in volcanic ash layers (Weinzierl et al., 2012). The lidar in Leipzig only probed the edges of the plume (Figs. 6, 11g–i), such that the observed particle backscatter coefficient β_{par} (up to 1 $Mm^{-1}\,sr^{-1}$) is most likely lower than that in the central part of the biomass burning aerosol layer. Using the observed particle backscatter coefficient, the optical thickness (532 nm) of the layer is estimated to be at least 0.15–0.20, which is in the range of previous findings for biomass burning aerosol layers, but higher than the median, of Weinzierl et al. (2011).

5.2 Comparison of the rBC mass concentrations and rBC size distributions with measurements in other biomass burning plumes

In the previous sections we showed that the Pagami Creek fire plume observed in the altitude range of 9–12 km on 16 September 2011 reached rBC mass concentrations between 0.03 $\mu g\,m^{-3}$ and 0.35 $\mu g\,m^{-3}$ (stp), which are comparable with the stp rBC mass concentration in the PBL over Neubrandenburg-Trollenhagen (0.11 $\mu g\,m^{-3}$ and 0.05 $\mu g\,m^{-3}$; stp) and Oberpfaffenhofen (0.38 $\mu g\,m^{-3}$ and 0.96 $\mu g\,m^{-3}$; stp) on that day but far larger than the background concentration (< 0.01 $\mu g\,m^{-3}$; stp) at the same altitude as the plume. Oberpfaffenhofen is located near the metropolitan area of Munich. Therefore these values are representative for a polluted PBL. To put the results of the observed forest fire plumes in context to the literature and to other typically expected BC-containing aerosol types, several papers are chosen: biomass burning plumes from Wyoming (Pratt et al., 2011); biomass burning from North America and Asia (Kondo et al., 2011a); biomass burning and anthropogenic emissions from California (Sahu et al., 2012); biomass burning and urban emissions from Texas (Schwarz et al., 2008a); urban emissions from California (Metcalf et al., 2012). Kondo et al. (2011a) measured

ACPD
13, 28751–28818, 2013

in 12–24 h old biomass burning plumes at altitudes from ground to roughly 5 km the highest rBC mass concentration in smoldering burning events (0.27–1.24 $\mu g\,m^{-3}$; stp). Sahu et al. (2012) observed rBC mass concentrations of $0.50 \pm 0.17\,\mu g\,m^{-3}$ (stp), while Pratt et al. (2011) reported total rBC mass concentrations of up to $2\,\mu g\,m^{-3}$ in fresh biomass burning plumes (~ 2–120 min old) in altitudes up to 3.5 km a.g.l. These concentrations are a factor of 5–60 larger than those found for the aged Pagami Creek smoke plume (3–4 days old) in this study. However, the measurements by Pratt et al. (2011) were taken in altitudes lower 3.5 km whereas our measurements were taken above 10 km. These differences, however, may be attributed at least partly to the dilution caused by turbulent mixing and wet removal processes. Besides the emissions of forest fires, preexisting BC particles originating from other sources such as traffic and other anthropogenic combustion processes may contribute to the BC load in forest fire plumes. However, due to the intensity and the remote location of the fire, this fraction is assumed to be small so that the described characteristics can be considered to be representative of the forest fire particles.

Besides the rBC mass concentration, the mass size distribution is an important aspect for rBC in the atmosphere. As can be seen from Fig. 9, the MMD in the Pagami Creek Plume is between 120 nm and 160 nm. These MMDs are smaller than observed by Kondo et al. (2011a) who found MMDs between 177 nm and 197 nm in fresh biomass burning plumes (age < 1 day, origin: North America) and between 176 nm and 238 nm in aged biomass burning plumes (age: 2–3 days, origin: Asia). MMDs in biomass burning plumes observed at altitudes between 0 km and 3.5 km a.g.l. in California by Sahu et al. (2012) are 193 ± 16 nm. Schwarz et al. (2008a) observed MMDs of roughly 160–180 nm for urban emissions and roughly 200–220 nm for biomass burning aerosol, while Metcalf et al. (2012) observed modes of roughly 120–140 nm for boundary layer aerosol and roughly 160 nm for free-tropospheric aerosol during airborne measurements in the Los Angeles Basin. Moteki et al. (2012) and Oshima et al. (2012) describe the wet removal of rBC during transport. A size-dependent wet removal (Moteki et al., 2012) can shift the MMD of aged BC layers towards smaller

ACPD
13, 28751–28818, 2013

particle sizes and might cause differences in observed MMDs for BC particle populations with varying exposure to wet removal conditions during the transport as potential reason for the observed differences. They observed, for instance, for the count median diameter a decrease from 127 nm to 97 nm with decreasing transport efficiency.

Pratt et al. (2011) observed with their SP2 average BC mass fractions of 0.3–34 % in fresh biomass burning plumes with the largest part of the mass (60–90 %) being non-refractory organic material. Comparably high mass fractions of organic material are also reported by Kondo et al. (2011a) who find an organic fraction of 56–92 % and a BC mass fraction of 1.7–4.9 %. The values from Kondo et al. (2011a) are comparable to findings from Sahu et al. (2012) presenting < 5 % BC mass fractions. The higher amount of OC compared to BC can be explained by emission factors, which are 0.2 g BC and 7.8 g OC per kg burned mass for boreal coniferous forests (McMeeking, 2008; Wiedinmyer et al., 2011). In our study, the volume fraction for rBC-containing particles derived from the SP2 for the 14 considered sequences is 2.5–3.9 % in the described size range. No measurements of organic material were performed but we have to assume that in our case OC is also a major constituent in terms of mass fraction.

5.3 Comparison of the total particle number size distributions with measurements in other biomass burning plumes

Figure 10 shows total aerosol number size distributions, including BC-free particles for the most part and a minor fraction of BC-containing particles, of the Pagami Creek fire plume in comparison to size distributions of biomass burning plumes published in previous studies. For the Pagami Creek plume, the median, maximum and minimum number size distribution is presented. The comparison of the biomass burning size distributions with measurements in clean UTLS "background" air exhibits one striking feature: the Aitken and accumulation modes give roughly comparable contributions to particle number concentration in the Pagami Creek fire cases, while the accumulation mode has a very minor contribution in the background case. On 16 September 2011, no particles larger than 400 nm were present in the background air, while particles up

ACPD
13, 28751–28818, 2013

to larger 1 µm were detected in the Pagami Creek plume. In all Pagami Creek smoke plume cases the accumulation mode is strongly enhanced compared to the background sample. Deviating from the monomodal structure of the background aerosol, the particles larger 0.14 µm can be attributed to the forest fire. The comparison of our results with number size distributions of biomass burning plumes from the SAMUM-2 field experiment at 0.8–4.2 km altitude (Weinzierl et al., 2011), SAFARI 2000 field experiment at roughly 2–5 km altitude (Haywood et al., 2003), the LACE 98 field experiment at 3–5 km altitude (Fiebig et al., 2003) and ICARTT-ITOP field experiment at 3–9 km altitude (Petzold et al., 2007) shows that in all biomass burning aerosol cases an enhanced accumulation mode is present. Especially in the ICARTT-ITOP case where a 6–9 days old Canadian forest fire aerosol layer over Europe was investigated, the bimodal structure of the size distribution is very pronounced and similar CMDs are found as in our case. Results from LACE 98 (Fiebig, 2001) exhibit a bimodal structure with similar CMDs as well with total number concentration about 2–9 times higher than in the Pagami Creek fire plume by approximating stp conditions (not shown). The SAMUM-2 case (3–6 days old) shows a similar CMD for particles > 0.14 µm but the mode for particles < 0.14 µm is not as enhanced compared to our results. In addition, Weinzierl et al. (2011) reported a significant coarse mode fraction for data collected during the SAMUM-2 field experiment attributable to mineral dust. In contrast we observed no significant amount of aerosol particles larger 1 µm. Results from SAFARI 2000 show only the accumulation mode since no measurements or extrapolations for particles < 100 nm were performed. Furthermore, the SAFARI 2000 size distribution was scaled to quantities found in our and the other studies, since in Haywood et al. (2003) the size distribution is given as normalized distribution. In summary, our observations are similar to biomass burning number size distributions observed previously especially for ICARTT-ITOP and LACE 98, indicating similar origins, source material, environmental and burning conditions or transportation. The layers often show similar modes in the accumulation mode size range, while the Aitken mode is observed less frequently in some cases possibly representing an aerosol, where the background aerosol might still dominate over the

ACPD
13, 28751–28818, 2013

biomass burning influence. Thus, a dominant accumulation mode and a relatively large modal diameter (~ 200–400 nm) seem to be common features of forest fire aerosols.

5.4 Coating thickness

Besides the size distribution information of aerosol layers, the mixing state of individual particles plays an important role in atmospheric processes. As described in Sect. 2.2, the coating thickness of individual particles inferred from the SP2 measurements delivers information about the mixing state of individual particles. Figure 12a shows normalized histograms of the observed coating thickness of all BC-containing particles with BC cores in the size range of rBC mass equivalent diameters between D_{rBC} = 140–160 nm and D_{rBC} = 180–220 nm for the 14 different sequences of measurements in the Pagami Creek fire plume. These two size ranges are chosen exemplarily to test if the coating thickness (Δ_{coat}) varies with changing BC core size. As it can be seen from Fig. 12a, the coating thickness of individual aerosol particles from the Pagami Creek aerosol layer ranges from Δ_{coat} = 20 nm up to > 180 nm, in both BC core size ranges shown, with a flat maximum between ~ 80 nm and 160 nm. The small number of BC cores with coatings below 20 nm observed within the forest fire plume are likely from UTLS background particles and/or aircraft emissions. The observed coating thickness distributions are very similar for all 14 sequences, indicating very homogeneous BC particle properties across the different plume areas.

For comparison, the rBC particles observed in the boundary layer in the regions of Neubrandenburg and Munich are thinly coated and show median coating thicknesses of < 20 nm with the majority (75-percentile) showing coating thicknesses less than 65 nm. Thus the particles in the observed aerosol layer exhibit much larger coating thicknesses than younger aerosol particle populations such as the PBL aerosol. The negative coating thickness values measured for some particles (Fig. 12a) are caused by random noise and potential systematic biases resulting from the assumptions made about the refractive indices and particle shape. The systematic uncertainty for the coating thickness is assessed to be < ±20 nm.

ACPD
13, 28751–28818, 2013

The raster graphic in Fig. 12b illustrates the relationship between the BC core size and the coating thickness integrated over all Pagami Creek fire plume sequences. The color-coding and the black line represent the number of particles in each pixel and the median coating thickness, respectively. The grey lines represent the detection limits of this method (see figure caption for explanation). Coating thickness values up to the detection limit, which is as high as $\Delta_{coat} \approx 240$ nm for core sizes $D_{rBC} \leq 100$ nm, are observed for all core sizes. The distribution of coating thickness values is similarly broad for all BC core sizes, but particles with thin coatings ($\Delta_{coat} \leq 40$ nm) are always a negligible fraction. The median coating thickness is $\Delta_{coat} \approx 105$–$136$ nm for the 14 flight sequences independent of BC core size (note, the median coating thickness values for BC core sizes $D_{rBC} < 90$ nm and > 170 nm are likely biased by detection limit effects). This translates to median shell/core diameter ratios of $D_{opt}/D_{rBC} = 3.7$, 2.8 and 2.4 at $D_{rBC} = 90$ nm, 130 nm and 170 nm, respectively, while the highest observed values are as high as $D_{opt}/D_{rBC} = 7.4$.

Akagi et al. (2012) found for a chaparral fire that 4 h after emission 85 % of the BC cores may have been thickly coated, i.e. with shell/core diameter ratios (D_{opt}/D_{rBC}) larger than approximately 2 whereas Kondo et al. (2011a) observed rBC particles in biomass burning plumes with shell/core ratios of $D_{opt}/D_{rBC} = 1.3$–1.6 in biomass burning plumes. These values are somewhat lower than our observations, which may be related to differences in the properties of the freshly emitted particles or continued mass acquisition of the BC particles during the long-range transport in the Pagami Creek forest fire plume. Anyway, the coatings reported for the BC particles from forest fires in all three studies discussed here are substantial. This is in contrast to BC particles emitted from diesel engines and wood burning for residential heating, which emit particles with very little and moderate coatings, respectively, and also the median coating thickness observed in aged aerosols typically remains clearly below 100 nm (Laborde et al., 2013 and references therein).

The very thick coatings of the BC particles in the forest fire plume will influence their light-absorption properties, as discussed in detail in Sect. 5.5. Furthermore, they

ACPD
13, 28751–28818, 2013

will also influence their interaction with clouds. They are expected to be good cloud condensation nuclei through the mere size effect as well as the additional hygroscopic water uptake by the coating (e.g. McMeeking et al., 2011; Laborde et al., 2013; Liu et al., 2013). Furthermore, the mixing state of the BC with organic and inorganic matter might have an influence on the ice nucleation efficiency of the particles and is thus relevant for the indirect aerosol effect (Hoose and Möhler, 2012).

5.5 Morphology and mixing state of BC particles

The interaction of BC-containing particles with solar radiation depends on their morphology and mixing state with light-scattering aerosol components (Kahnert et al., 2012). The coating thickness values reported in the previous section were inferred assuming a concentric-spheres core-shell morphology for the BC core and a light-scattering coating. However, the BC cores of combustion particles are fractal-like or compact aggregates and the BC can be mixed with light-scattering material in different manners, including e.g. surface contact of the BC with the light-scattering components, full immersion of the BC in the light-scattering component or immersion of the light-scattering components in the BC aggregate (Scarnato et al., 2013). Previous laboratory and field experiments have shown that the SP2 signals of BC-containing particles can sometimes give indirect evidence of how the BC core is mixed with the light-scattering components beyond just quantifying the coating thickness (Sedlacek et al., 2012; Moteki and Kondo, 2007).

Figure 13 schematically shows the particle-laser interaction of different particle types and the corresponding SP2 signals including the time-resolved scattering cross-section as inferred from the raw LSD signal according to the method described in Laborde et al. (2012a). For BC-free particles (Fig. 13a) the LSD signal usually follows an almost Gaussian shape. The LSD signal is directly proportional to the laser intensity profile along the flight path of the particle through the laser beam, because the size and thus also the scattering cross-section of a non-absorbing particle remains unchanged during

ACPD
13, 28751–28818, 2013

laser transition. The maximum of the LSD signal from BC-free particles occurs at the center of the laser beam (here at time 128 · 0.2 µs; Fig. 13a).

In contrast the size of a BC-containing particle is reduced during laser transition, first through evaporation of non-refractory coating material followed by evaporation of BC, which has a higher boiling point. Figure 13b shows typical SP2 signals of a BC-containing particle with a medium thick coating. The LSD responds with an increasing signal when the particle enters the laser beam and scatters the laser light with a constant scattering cross-section. Travelling further into the laser beam, the BC core absorbs the laser radiation and heats up. As a consequence, the coating evaporates and causes a decrease in the scattering cross-section. This often results in a first local maximum of the LSD signal (here at time 103 · 0.2 µs; Fig. 13b). After complete evaporation of the coating, the scattering cross-section of the particle stabilizes for a short time and the LSD signal raises again, because the laser intensity still increases (time range 112 · 0.2–116 · 0.2 µs; Fig. 13b). The BC core heats up further until it reaches the boiling point of BC. The thermal radiation, emitted by the particle and detected by the incandescence detectors, now reaches its maximum (here at time 119 · 0.2 µs; Fig. 13b), and the BC core evaporates, resulting in a fast decrease of the BC mass and thus also the scattering cross-section of the residual particle, which is reflected in a fast decrease of the BID and LSD signals, respectively. Consequently, the LSD signal can have a second local maximum around the peak of the BID signal (here at time 115 · 0.2 µs; Fig. 13b). This second local maximum is typically higher than the first local maximum of the LSD signal for BC particles with a thin or medium coating, such that the global maximum of the LSD signal occurs about at the same time as the peak of the BID signal. For thickly coated BC particles, the first local maximum of the LSD signal is typically higher than the second local maximum, such that the global maximum occurs before the peak of the BID signal. Moteki and Kondo (2007) have shown that the time lag between the peaks of the LSD and the BID signals gives a crude information about the mixing state of BC-containing particles, where values $> \sim 2$ µs are associated with thick coatings, while values $< \sim 2$ µs are associated with thin to medium coatings.

ACPD
13, 28751–28818, 2013

However, in the literature also particles that disintegrate in the laser beam of the SP2 have been reported (Moteki and Kondo, 2007; Sedlacek et al., 2012). Disintegration occurs before the BC core reaches its boiling point and results in a BC-free fragment, which remains stable after disintegration, and a BC fragment that eventually evaporates. Figure 13c shows the SP2 signals of such a disintegrating BC-containing particle. Disintegration can be identified by the fact that the LSD signal does not fully disappear after evaporation of the BC core. More precisely, the scattering cross-section stabilizes again after the peak BID signal, as the BC-free fragment does not evaporate any further (here at time $> 120 \cdot 0.2\,\mu s$; Fig. 13c). Furthermore, the stabilization of the measured scattering cross-section after the peak BID signal is a key feature that distinguishes disintegrating particles from coincidence of a BC-containing and a BC free particle. The BC-free fragment from a disintegrated particle, which behaves as a BC-free particle after its separation, causes another local maximum of the LSD signal at the center of the laser beam (here at time $139 \cdot 0.2\,\mu s$; Fig. 13c). This local maximum of the LSD signal from the BC-free fragment can be the global maximum, if the BC-free fragment is a substantial portion of the original particle. In this case the time lag between the peaks of the LSD and the BID signals becomes negative as the peak of the BID signal normally occurs before the center of the laser beam.

Sedlacek et al. (2012) have reported the identification of disintegrating particles through negative lagtimes for the first time. However, in our study, only a minor fraction of all disintegrating particles could be identified via a negative lagtime, because most of the disintegrating particles either exhibited a positive lag time or because the peak of the LSD signal and with that also the lagtime were not defined due to LSD detector saturation. Therefore, the time-dependent (position-dependent) scattering cross-section, as inferred from the raw LSD signal, according to the method described in Laborde et al. (2012a), was used here to identify disintegrating particles. Specifically, the scattering cross-section measured in the trailing-edge of the laser beam (at the position with 3 % of the maximum laser power) was used to determine for all BC-containing particles whether a detectable BC-free fragment, producing an LSD signal above background

ACPD
13, 28751–28818, 2013

noise, remained left in the trailing-edge of the laser beam. The scattering cross-section measured in the leading-edge of the laser beam (at the position with 3 % of the maximum laser power) was used to determine the size of the undisturbed particles, in order to further investigate the influence of particle size on disintegration. The trailing-edge LSD signal indicates that about 50 % of the BC-containing particles with particle size of about D_{opt} = 300 nm disintegrated in the laser beam, leaving a detectable BC-free fragment. The fraction of disintegrating particles increased with increasing particle size, so that > 90 % of the BC particles disintegrated at large sizes (D_{opt} >∼ 480 nm). Conversely, the majority of the smaller particles (D_{opt} <∼ 300 nm) showed no disintegration characteristics. However it cannot be distinguished if they really evaporate completely or if potential BC-free fragments just remain below the detection limit of the LSD. Overall ∼ 40–50 % of all detected BC-containing particles were identified as disintegrating particles with the trailing-edge LSD signal method. Only 3.5–6.8 % (median: 4.6 %) of all BC particles, corresponding to roughly 5–20 % of all identified disintegrating BC particles, exhibited a negative lagtime in this study. This shows that the lagtime method only provides a lower limit for the total fraction of disintegrating particles. The success rate of the lagtime method for the identification of disintegrating particles depends on particle and instrument properties such as e.g. the particle size and the saturation level of the LSD.

Sedlacek et al. (2012) observed disintegrating particles during a ground-based field campaign in summer 2011. More than 60 % of BC-containing particles in the forest fire aerosol plume from several wildfires east of Lake Winnipeg and into western Ontario on 30 July were disintegrating BC particles, exhibiting negative lagtimes in the SP2. Our observations show for the first time the occurence of disintegrating BC particles in high-altitude BC layers (40–50 % of all detected BC-containing particles, according to the trailing-edge LSD signal method).

Sedlacek et al. (2012) suggested that disintegrating particles are associated with a particular particle morphology, where the BC is located near or at the surface of the BC-containing particles. Moteki and Kondo (2007) also reported the occurrence of

ACPD
13, 28751–28818, 2013

disintegrating particles in laboratory experiments with graphitic cores that were coated with glycerol or oleic acid. The number fraction of disintegrating particles was mainly a function of overall particle diameter. No disintegration was observed for small sizes, while almost all larger particles disintegrated. The threshold particle diameter for the occurrence of disintegration was 450–600 nm depending on the coating type. Moteki and Kondo (2007) speculated that disintegration might be associated with eccentrically positioned BC cores in their case, while near-surface BC morphology was not expected based on the process applied to coat the BC cores.

The specific BC particle morphology, i.e. core-shell vs. near-surface BC, is relevant because the light-absorption efficiency enhancement effect by light-scattering coatings internally mixed with BC depends on the coating volume fraction as well as the particle morphology. Coatings with D_{opt}/D_{rBC}-ratios of 2 can already enhance the light-absorption by the BC cores by 100 % (Schwarz et al., 2008b; Shiraiwa et al., 2010), while the relation between the coating thickness and the enhancement factor is not linear and saturation occurs above a certain threshold. The high D_{opt}/D_{rBC}-ratios observed in the Pagami Creek forest fire plume imply that substantial light-absorption enhancement effects are expected, though large uncertainties of this effect remain (e.g. Cappa et al., 2012). Sketches of three conceivable morphologies of disintegrating BC-containing particles are shown in Fig. 13c (on the very left): concentric core-shell, eccentric core-shell or near-surface BC/attached BC morphology. Light-scattering matter that is simply attached to a BC core causes very little enhancement of the light-absorption efficiency (Liu and Mishchenko, 2007; Scarnato et al., 2013). In contrast, a substantial light-absorption efficiency enhancement can be expected for coated BC-containing particles with a concentrically or eccentrically positioned core. Besides, disintegrating particles might also complicate the analysis of SP-AMS (Soot-Particle Aerosol Mass Spectrometer; Onasch et al., 2012) measurements, because the BC-free fragment would not be evaporated by the laser. This should be further investigated with specific laboratory experiments involving biomass burning aerosol and the SP-AMS.

ACPD
13, 28751–28818, 2013

A process that can produce near-surface BC morphologies is coagulation of almost bare BC aggregates with BC-free particles. Condensation of secondary organic or inorganic aerosol components on BC particles can either result in particles with core-shell morphology (concentric or eccentric) or with near-surface BC morphology. Adachi et al. (2010) proposed a mechanism producing near-surface BC particles via condensation processes, which involves condensation of organic material onto nascent BC that effectively preserves the aggregate of primary BC particles in an un-collapsed form, followed by further mass acquisition via condensation preferentially onto the more organic portion of the particle. Based on our observations in the aged Pagami Creek smoke plume, disintegration was associated with large BC-containing particles (overall optical diameter $>\sim 300$ nm; see above). These large particles generally had a very low rBC mass fraction since the majority of the rBC cores were < 130 nm in diameter. They can be the result of extensive condensation of secondary aerosol components onto the nascent BC aggregates or of coagulation of BC-particles with large BC-free particles during transport. Indeed, the initial plume was highly concentrated such that both processes are likely to occur during aging of the BC particles in the plume. Thus, it is in principle possible that both BC particle types with near-surface BC or core-shell morphology are present in the aged plume. However, the observed number fraction of disintegrating particles is for the most part a function of overall particle size, indicating that disintegration was possibly just the result of very thick coatings, as reported in the laboratory study by Moteki and Kondo (2007). Specific evidence neither to corroborate nor to discard the assumption of near-surface BC morphology is available.

The particular features of the particles in the aged Pagami Creek fire plume observed in this study are the enhanced size of all particles (Fig. 10) and the enhanced coating thickness of BC-containing particles (Fig. 12a) compared to the observations outside the plume. Both can be attributed to extensive coagulation and/or condensation in the forest fire plume. It is important to consider the large particle size when assessing the radiative impact of such plumes by direct light-scattering of solar radiation. When assessing the radiative impact via absorption of solar radiation, it is recommended,

ACPD
13, 28751–28818, 2013

based on above discussion about the morphology of BC particles, to consider the light-absorption enhancement effect that is expected to occur for thickly coated BC particles with core-shell morphology.

The first two reports of disintegrating BC particles in ambient aerosols are from forest fire plumes (Sedlacek et al., 2012 and this study). The question if disintegrating particles are uniquely or predominantly associated with biomass burning aerosol remains to be addressed. A UTLS background sequence on 16 September 2011 showed an insignificant amount of disintegrating particles (< 1 %). The fact, that biomass burning BC-particles often exhibit thicker coatings compared to BC particles from e.g. diesel engines, even with allowance for coating acquisition during atmospheric aging (e.g. Laborde et al., 2013), might be a reason for preferential occurrence of disintegrating particles in biomass burning aerosol.

5.6 Black carbon import into the UTLS by the Pagami Creek fire in comparison to aviation

In this section we present two estimates to determine the primary emissions from the Pagami Creek fire (first approach) and the import of BC from the fire to the UTLS region (second approach).

The first approach applied here estimates the total OC and BC emissions based on the burnt area, wood mass per area and emission factor for boreal needleleaf forests. For this rough estimate of the BC and OC mass directly emitted by the Pagami Creek fire (Fig. 14a) values presented in Wiedinmyer et al. (2011) are used: BC and OC emission factors for boreal coniferous forests (0.2 g per kg biomass burned and 7.8 g per kg biomass burned, respectively; McMeeking, 2008) and fuel loadings for North American boreal forests (25 kg m^{-2}; Akagi et al., 2011 and references therein) are combined with the burned area (~ 350 km^2; US Forest Service), resulting in roughly 2×10^3 Mg BC and 68×10^3 Mg OC emitted from the Pagami Creek fire. This estimate is strongly linked to the assumptions made for the burned area and the applied emission factors and needs to be considered with caution as empirical estimate, implying large

ACPD
13, 28751–28818, 2013

uncertainties. However large parts of these primary emissions will fall out quickly, by e.g. wet deposition (see 5.2), or will be transported at altitudes below 8 km (see Fig. 3; Mattis et al., 2008; Weinzierl et al., 2011) or will not enter the free troposphere. The fraction of the emissions entering the upper troposphere is more relevant in terms of its impact on the radiation budget due to lower washout rates associated with longer life times and the possibility of long-range transport.

In order to assess the BC import of the Pagami Creek fire to the UTLS, the second approach uses the measurements in the plume and the plume dispersion modeling (HYSPLIT) to estimate the BC import of the Pagami Creek fire plume to the UTLS region above Europe. Assuming a homogeneously distributed aerosol layer, we approximately can derive the BC mass import from the Pagami Creek fire event into the UTLS region above Europe (Fig. 14b) from our measurements and dispersion model simulations. The area of the aerosol layer is deduced from the HYSPLIT dispersion calculation by sizing the plume area for 15 September 2011 (20:00–23:00 UTC) representative for the plume observed 12 h later above Europe by assuming a plume concentration threshold (0.1 a.u.; see Fig. 11) and a rational uncertainty (area: $(3 \pm 2) \times 10^5$ km^2; Sect. 4), based on the similarity of the dispersion calculation and observations from IASI (Sect. 4) and GOME (Sect. 5.1). The height of the aerosol layer is deduced from the lidar observations (height: 2 ± 1 km; Sect. 3.2). Thus, the volume of the plume is derived (1×10^5–1.5×10^6 km^3; best estimate: 6×10^5 km^3). As BC mass concentration we use the rBC mass concentration from our measurements in the edge of the plume (7–84 ng m^{-3}; median of measurement sequences: 42 ng m^{-3}; at ambient conditions). From these data we obtain a best estimate for the BC total mass import to the high-altitude aerosol layer above Europe of 25 Mg (i.e. tons) BC, ranging from 1–126 Mg BC. This estimate depends strongly on the assumed duration of the emission, because e.g. a shorter duration would decrease the area covered by the plume of the dispersion calculations at the time of measurements. Nevertheless, we showed (Sect. 4) that the chosen duration of the emissions is in good agreement with observations of the duration of the fire. The local inhomogeneities observed both in simulation (Fig. 11) as well

ACPD
13, 28751–28818, 2013

as in measurement (Fig. 4) cause a large uncertainty in both the plume area as well as the average concentration. However, the uncertainties of this estimate are smaller compared to the theoretical estimate on the direct total emissions of the Pagami Creek fire described above, because the input parameters are based on direct measurements and calculations related to the specific event compared to generalized emission factors used in the first approach. Since the dispersion calculation suggests that the measurements took place in the less-concentrated tail of the plume the maximum value of 126 Mg BC might still be an underestimation of the imported BC mass. However, it is highly probable that the real BC mass of the Pagami Creek fire plume ranges within in the presented span of 1–126 Mg BC.

Comparing the direct emissions at the source with the plume observed above Europe and taking into account the given uncertainties due to the assumptions, e.g. for plume distribution calculation and emission factors, and that we consider only the plume transported to Europe in altitudes above 10 km, the extended aerosol layer above Europe on 16 September 2011 contains < 7 % of the BC mass emitted from the fire. This is reasonable agreement, keeping in mind that both estimates contain considerable uncertainties and that the second approach only estimates the portion of the emissions that remains in the atmosphere after 4 days of long-range transport at high altitudes whereas the estimate based on the first approach is for the total direct BC emissions. However, the reasonable agreement between the two independent estimates gives better trust in these numbers.

These estimates show that singular forest fire events can be a relevant source for the BC loadings in the UTLS region on the time scale of at least days. Besides forest fires, another (permanent) source for BC in the UTLS region are emissions from aircraft (Fig. 14c). Aviation emissions are estimated by Lee et al. (2010) to be 16 $\mathrm{Mg\,d^{-1}}$ soot (defined as BC + OC). The BC/OC ratio for aviation-induced soot emissions is roughly 3.5 (Bond et al., 2004, and references therein). Thus, the aviation-induced soot emission value of Lee et al. (2010) can be converted to roughly 12 $\mathrm{Mg\,d^{-1}}$ (BC). Bond et al. (2013) estimate the aviation-induced BC to be 55 $\mathrm{Mg\,d^{-1}}$ BC. The BC emis-

ACPD
13, 28751–28818, 2013

sions from aviation to the UTLS region are even smaller, taking into account that the total aviation-induced emissions contain also emissions during take-off and landing to lower altitudes. Nevertheless, the best guess of the BC mass imported from the Pagami Creek fire to the UTLS region over Europe after several days of transport is the same magnitude as the daily globally averaged BC mass emission of aviation. The comparison of 1–126 Mg BC in the Pagami Creek fire plume in the UTLS region over Europe to 12–55 Mg d^{-1} BC related to aviation shows the relevance of such singular forest fire events as a source for the import of black carbon into the atmosphere. A future increase in forest fire events might be of great importance on the BC import into the upper troposphere. However, this result is based on several assumptions. Therefore the given values should be considered with caution as rough estimated values but should illustrate the potential relevance of forest fires as a source for BC in the UTLS region.

6 Summary and conclusion

In the framework of the CONCERT 2011 field experiment we observed an intense elevated forest fire aerosol layer over northeast Germany with the DLR research aircraft Falcon on 16 September 2011 between 10 km and 12 km altitude. This layer was characterized using aerosol airborne in-situ measurements and a ground-based lidar (TROPOS Leipzig). The vertical profiles for the flights on 16 September showed the intensity of the described aerosol layer. The median vertical profile for the entire CONCERT 2011 field experiment represents an estimate for the typical black carbon mass mixing ratio in September for Mid-Europe and allowed classifying the Pagami Creek fire plume with respect to this average situation. Dispersion simulations with HYSPLIT help to identify the source of the aerosol layer.

To obtain information about the aerosol layer characteristics, refractory black carbon (rBC) mass size distributions and total aerosol particle number size distributions were calculated for different sequences in the heterogeneous Pagami Creek fire plume. The

ACPD
13, 28751–28818, 2013

mode parameters of the applied log-normal fits were compared to size distributions of biomass burning aerosol from other studies. To determine the impact of those plumes on the radiation budget it is essential to investigate the mixing state of the particles. Therefore, the coating thickness of individual aerosol particles was calculated, assuming ideal-spherical BC particles coated with a non-absorbing material. Besides that, we delivered information about the mixing structure of individual particles, more precisely whether an BC-containing particle disintegrates in the SP2 laser beam. This was found recently in ground-based measurements of forest fire aerosol and now is for the first time confirmed for airborne in-situ measurements of forest fire aerosol plumes.

In summary, the major findings of this study are:

- The aerosol layer observed on 16 September 2011 in the UTLS over Germany is attributed to the Pagami Creek fire in Minnesota, USA, supported among other observations by the measured lidar linear depolarization ratio (532 nm) of 6–8 %, indicating a forest fire source.
- The total rBC mass concentration of the aged (3–4 days old) Pagami Creek smoke plume ranges from 0.03–0.35 $\mu g\,m^{-3}$ (stp), comparable to rBC mass concentrations typical for moderately polluted planetary boundary layers. The MMDs of the rBC size distribution range between 120 nm and 160 nm.
- In contrast to a background air sample showing a monomodal number size distribution, the Pagami Creek fire plume shows a bimodal number size distribution with a pronounced accumulation and Aitken mode.
- The rBC particles in the Pagami Creek fire plume show coating thicknesses of roughly 50–220 nm with a maximum between ~ 80 nm and 160 nm (median: 105–136 nm), whereas fresh PBL aerosol exhibits coatings predominantly < 65 nm (median: < 20 nm). Most likely the coating consists of a mix of organic and inorganic species, which has an impact on the rBC radiative forcing, on the rBC hygroscopicity, and on the efficiency to act as cloud condensation or ice nu-

ACPD
13, 28751–28818, 2013

clei. Resulting from small rBC diameters and large coating thicknesses, we observe shell/core ratios of up to 7.4 with median shell/core diameter ratios of D_{opt}/D_{rBC} = 3.7, 2.8 and 2.4 at D_{rBC} = 90 nm, 130 nm and 170 nm, respectively.

– We show that the majority of the rBC-containing particles disintegrate in the SP2 laser beam. This process is an indication of very thickly coated rBC cores or rBC cores located eccentrically, near the surface or at the surface of rBC-free particles. The observed number fraction of disintegrating particles is for the most part a function of overall particle size, indicating that disintegration was possibly just the result of very thick coatings. The question if disintegrating particles are uniquely or predominantly associated with biomass burning aerosol remains to be addressed. The fact, that biomass burning BC-particles often exhibit thick coatings might be a reason for preferential occurrence of disintegrating particles in biomass burning aerosol.

– We present a rough estimate of the BC mass import due to the Pagami Creek fire to the UTLS region above Europe (best estimate: 25 Mg BC) and compare it with the daily BC emissions of global aviation (12–55 Mg BC) and thereby highlight the relevance of forest fires to act as a potential BC source for the upper free troposphere.

In conclusion, the microphysical properties of the observed extended Pagami Creek fire plume obtained within this case study clarify the relevance of pyro-convection as particle source and as source for long-range transport of forest fire aerosol layers in the UTLS region. The highly variable particle composition, mixing state, and concentrations increase the heterogeneity of biomass burning plumes. This has a manifold of impacts on the radiation budget of the atmosphere, which are not yet fully understood. Consequently, this study enables to assess the impact of light-absorbing aerosol layers on the radiation budget using radiation transfer calculations. To globalize the BC mass import into the upper troposphere and to minimize uncertainties of model estimates, additional in-situ measurements of aerosol layers similar to the presented layer

ACPD
13, 28751–28818, 2013

and additional studies of the processes of aerosol transport by pyro-convection to the UTLS region are necessary.

Acknowledgements. This work was funded by the Helmholtz Association under grant number VH-NG-606 (Helmholtz-Hochschul-Nachwuchsforschergruppe AerCARE). C. V. thanks funding by the Helmholtz Association under grant number VH-NG-309. The field experiment was performed within the DLR project CATS. The authors gratefully acknowledge NASA/GSFC, Rapid Response team for generation of the MODIS picture, NOAA Air Resources Laboratory (ARL) for the provision of the HYSPLIT transport and dispersion model and/or READY website (http://ready.arl.noaa.gov) used in this publication, NASA Langley Research Center Atmospheric Science Data Center for providing CALIPSO data, Ether CNES/CNRS-INSU Ether web site http://www.pole-ether.fr for providing the IASI CO information, and KNMI for providing the data of the GOME-2 Absorbing Aerosol Index in the framework of the EUMETSAT Satellite Application Facility on Ozone and Atmospheric Chemistry Monitoring (O3M SAF).

The service charges for this open access publication have been covered by a Research Centre of the Helmholtz Association.

References

Adachi, K., Chung, S. H., and Buseck, P. R.: Shapes of soot aerosol particles and implications for their effects on climate, J. Geophys. Res.-Atmos., 115, D15206, doi:10.1029/2009jd012868, 2010.

Akagi, S. K., Yokelson, R. J., Wiedinmyer, C., Alvarado, M. J., Reid, J. S., Karl, T., Crounse, J. D., and Wennberg, P. O.: Emission factors for open and domestic biomass burning for use in atmospheric models, Atmos. Chem. Phys., 11, 4039–4072, doi:10.5194/acp-11-4039-2011, 2011.

Akagi, S. K., Craven, J. S., Taylor, J. W., McMeeking, G. R., Yokelson, R. J., Burling, I. R., Urbanski, S. P., Wold, C. E., Seinfeld, J. H., Coe, H., Alvarado, M. J., and Weise, D. R.: Evolution of trace gases and particles emitted by a chaparral fire in California, Atmos. Chem. Phys., 12, 1397–1421, doi:10.5194/acp-12-1397-2012, 2012.

ACPD

13, 28751–28818, 2013

Andreae, M. O. and Gelencsér, A.: Black carbon or brown carbon? The nature of light-absorbing carbonaceous aerosols, Atmos. Chem. Phys., 6, 3131–3148, doi:10.5194/acp-6-3131-2006, 2006.

Andreae, M. O., Rosenfeld, D., Artaxo, P., Costa, A. A., Frank, G. P., Longo, K. M., and Silva-Dias, M. A. F.: Smoking rain clouds over the Amazon, Science, 303, 1337–1342, doi:10.1126/science.1092779, 2004.

Aquila, V., Hendricks, J., Lauer, A., Riemer, N., Vogel, H., Baumgardner, D., Minikin, A., Petzold, A., Schwarz, J. P., Spackman, J. R., Weinzierl, B., Righi, M., and Dall'Amico, M.: MADE-in: a new aerosol microphysics submodel for global simulation of insoluble particles and their mixing state, Geosci. Model Dev., 4, 325–355, doi:10.5194/gmd-4-325-2011, 2011.

Barnaba, F., Angelini, F., Curci, G., and Gobbi, G. P.: An important fingerprint of wildfires on the European aerosol load, Atmos. Chem. Phys., 11, 10487–10501, doi:10.5194/acp-11-10487-2011, 2011.

Bauer, S. E., Menon, S., Koch, D., Bond, T. C., and Tsigaridis, K.: A global modeling study on carbonaceous aerosol microphysical characteristics and radiative effects, Atmos. Chem. Phys., 10, 7439–7456, doi:10.5194/acp-10-7439-2010, 2010.

Baumgardner, D., Popovicheva, O., Allan, J., Bernardoni, V., Cao, J., Cavalli, F., Cozic, J., Diapouli, E., Eleftheriadis, K., Genberg, P. J., Gonzalez, C., Gysel, M., John, A., Kirchstetter, T. W., Kuhlbusch, T. A. J., Laborde, M., Lack, D., Müller, T., Niessner, R., Petzold, A., Piazzalunga, A., Putaud, J. P., Schwarz, J., Sheridan, P., Subramanian, R., Swietlicki, E., Valli, G., Vecchi, R., and Viana, M.: Soot reference materials for instrument calibration and intercomparisons: a workshop summary with recommendations, Atmos. Meas. Tech., 5, 1869–1887, doi:10.5194/amt-5-1869-2012, 2012.

Bond, T. C., Streets, D. G., Yarber, K. F., Nelson, S. M., Woo, J. H., and Klimont, Z.: A technology-based global inventory of black and organic carbon emissions from combustion, J. Geophys. Res.-Atmos., 109, D14203, doi:10.1029/2003jd003697, 2004.

Bond, T. C., Doherty, S. J., Fahey, D. W., Forster, P. M., Berntsen, T., DeAngelo, B. J., Flanner, M. G., Ghan, S., Kärcher, B., Koch, D., Kinne, S., Kondo, Y., Quinn, P. K., Sarofim, M. C., Schultz, M. G., Schulz, M., Venkataraman, C., Zhang, H., Zhang, S., Bellouin, N., Guttikunda, S. K., Hopke, P. K., Jacobson, M. Z., Kaiser, J. W., Klimont, Z., Lohmann, U., Schwarz, J. P., Shindell, D., Storelvmo, T., Warren, S. G., and Zender, C. S.: Bounding the role of black carbon in the climate system: a scientific assessment, J. Geophys. Res.-Atmos., 118; 5380–5552, doi:10.1002/jgrd.50171, 2013.

ACPD
13, 28751–28818, 2013

Buseck, P. R. and Posfai, M.: Airborne minerals and related aerosol particles: effects on climate and the environment, P. Natl. Acad. Sci. USA, 96, 3372–3379, doi:10.1073/pnas.96.7.3372, 1999.

Cappa, C. D., Onasch, T. B., Massoli, P., Worsnop, D. R., Bates, T. S., Cross, E. S., Davidovits, P., Hakala, J., Hayden, K. L., Jobson, B. T., Kolesar, K. R., Lack, D. A., Lerner, B. M., Li, S.-M., Mellon, D., Nuaaman, I., Olfert, J. S., Petaja, T., Quinn, P. K., Song, C., Subramanian, R., Williams, E. J., and Zaveri, R. A.: Radiative absorption enhancements due to the mixing state of atmospheric black carbon, Science, 337, 1078–1081, doi:10.1126/science.1223447, 2012.

Damoah, R., Spichtinger, N., Forster, C., James, P., Mattis, I., Wandinger, U., Beirle, S., Wagner, T., and Stohl, A.: Around the world in 17 days - hemispheric-scale transport of forest fire smoke from Russia in May 2003, Atmos. Chem. Phys., 4, 1311–1321, doi:10.5194/acp-4-1311-2004, 2004.

Damoah, R., Spichtinger, N., Servranckx, R., Fromm, M., Eloranta, E. W., Razenkov, I. A., James, P., Shulski, M., Forster, C., and Stohl, A.: A case study of pyro-convection using transport model and remote sensing data, Atmos. Chem. Phys., 6, 173–185, doi:10.5194/acp-6-173-2006, 2006.

de Graaf, M., Stammes, P., Torres, O., and Koelemeijer, R. B. A.: Absorbing aerosol index: sensitivity analysis, application to GOME and comparison with TOMS, J. Geophys. Res.-Atmos., 110, D01201, doi:10.1029/2004JD005178, 2005.

Diehl, T., Heil, A., Chin, M., Pan, X., Streets, D., Schultz, M., and Kinne, S.: Anthropogenic, biomass burning, and volcanic emissions of black carbon, organic carbon, and SO_2 from 1980 to 2010 for hindcast model experiments, Atmos. Chem. Phys. Discuss., 12, 24895–24954, doi:10.5194/acpd-12-24895-2012, 2012.

Draxler, R. R. and Hess, G. D.: Description of the HYSPLIT_4 modelling system, NOAA Technical Memorandum ERL ARL-224, Air Resources Laboratory, Silver Spring, Maryland, 1997.

Draxler, R. R. and Hess, G. D.: An overview of the HYSPLIT_4 modelling system for trajectories, dispersion, and deposition, Aust. Meteorol. Mag., 47, 295–308, 1998.

Fernald, F. G.: Analysis of atmospheric lidar observations: some comments, Appl. Optics, 23, 652–653, doi:10.1364/AO.23.000652, 1984.

Fiebig, M.: Das troposphaerische Aerosol in mittleren Breiten – Mikrophysik, Optik und Klimaantrieb am Beispiel der Feldstudie LACE 98, Ph.D. thesis, Fakultät für Physik, Ludwig-Maximilians-Universität München, Oberpfaffenhofen, 259 pp., 2001.

ACPD
13, 28751–28818, 2013

Fiebig, M., Stohl, A., Wendisch, M., Eckhardt, S., and Petzold, A.: Dependence of solar radiative forcing of forest fire aerosol on ageing and state of mixture, Atmos. Chem. Phys., 3, 881–891, doi:10.5194/acp-3-881-2003, 2003.
Fromm, M., Bevilacqua, R., Servranckx, R., Rosen, J., Thayer, J. P., Herman, J., and Larko, D.: Pyro-cumulonimbus injection of smoke to the stratosphere: observations and impact of a super blowup in northwestern Canada on 3–4 August 1998, J. Geophys. Res.-Atmos., 110, D08205, doi:10.1029/2004JD005350, 2005.
Fromm, M., Lindsey, D. T., Servranckx, R., Yue, G., Trickl, T., Sica, R., Doucet, P., and Godin-Beekmann, S. E.: The untold story of pyrocumulonimbus, B. Am. Meteorol. Soc., 91, 1193–1209, doi:10.1175/2010bams3004.1, 2010.
Gao, R. S., Schwarz, J. P., Kelly, K. K., Fahey, D. W., Watts, L. A., Thompson, T. L., Spackman, J. R., Slowik, J. G., Cross, E. S., Han, J. H., Davidovits, P., Onasch, T. B., and Worsnop, D. R.: A novel method for estimating light-scattering properties of soot aerosols using a modified single-particle soot photometer, Aerosol Sci. Tech., 41, 125–135, doi:10.1080/02786820601118398, 2007.
Groß, S., Esselborn, M., Weinzierl, B., Wirth, M., Fix, A., and Petzold, A.: Aerosol classification by airborne high spectral resolution lidar observations, Atmos. Chem. Phys., 13, 2487–2505, doi:10.5194/acp-13-2487-2013, 2013.
Haywood, J. M., Osborne, S. R., Francis, P. N., Keil, A., Formenti, P., Andreae, M. O., and Kaye, P. H.: The mean physical and optical properties of regional haze dominated by biomass burning aerosol measured from the C-130 aircraft during SAFARI 2000, J. Geophys. Res.-Atmos., 108, 8473, doi:10.1029/2002JD002226, 2003.
Hoose, C. and Möhler, O.: Heterogeneous ice nucleation on atmospheric aerosols: a review of results from laboratory experiments, Atmos. Chem. Phys., 12, 9817–9854, doi:10.5194/acp-12-9817-2012, 2012.
Jacobson, M. Z.: Strong radiative heating due to the mixing state of black carbon in atmospheric aerosols, Nature, 409, 695–697, doi:10.1038/35055518, 2001.
Jeßberger, P., Voigt, C., Schumann, U., Sölch, I., Schlager, H., Kaufmann, S., Petzold, A., Schäuble, D., and Gayet, J.-F.: Aircraft type influence on contrail properties, Atmos. Chem. Phys. Discuss., 13, 13915–13966, doi:10.5194/acpd-13-13915-2013, 2013.
Jost, H. J., Drdla, K., Stohl, A., Pfister, L., Loewenstein, M., Lopez, J. P., Hudson, P. K., Murphy, D. M., Cziczo, D. J., Fromm, M., Bui, T. P., Dean-Day, J., Gerbig, C., Mahoney, M. J., Richard, E. C., Spichtinger, N., Pittman, J. V., Weinstock, E. M., Wilson, J. C., and Xueref, I.:

ACPD
13, 28751–28818, 2013

In-situ observations of mid-latitude forest fire plumes deep in the stratosphere, Geophys. Res. Lett., 31, L11101, doi:10.1029/2003gl019253, 2004.

Jurkat, T., Voigt, C., Arnold, F., Schlager, H., Aufmhoff, H., Schmale, J., Schneider, J., Lichtenstern, M., and Doernbrack, A.: Airborne stratospheric ITCIMS measurements of SO_2, HCl, and HNO_3 in the aged plume of volcano Kasatochi, J. Geophys. Res.-Atmos., 115, D00L17, doi:10.1029/2010JD013890, 2010.

Kahnert, M., Nousiainen, T., Lindqvist, H., and Ebert, M.: Optical properties of light absorbing carbon aggregates mixed with sulfate: assessment of different model geometries for climate forcing calculations, Opt. Express, 20, 10042–10058, doi:10.1364/OE.20.010042, 2012.

Klett, J. D.: Stable analytical inversion solution for processing lidar returns, Appl. Optics, 20, 211–220, doi:10.1364/ao.20.000211, 1981.

Knorr, W., Lehsten, V., and Arneth, A.: Determinants and predictability of global wildfire emissions, Atmos. Chem. Phys., 12, 6845–6861, doi:10.5194/acp-12-6845-2012, 2012.

Kondo, Y., Matsui, H., Moteki, N., Sahu, L., Takegawa, N., Kajino, M., Zhao, Y., Cubison, M. J., Jimenez, J. L., Vay, S., Diskin, G. S., Anderson, B., Wisthaler, A., Mikoviny, T., Fuelberg, H. E., Blake, D. R., Huey, G., Weinheimer, A. J., Knapp, D. J., and Brune, W. H.: Emissions of black carbon, organic, and inorganic aerosols from biomass burning in North America and Asia in 2008, J. Geophys. Res.-Atmos., 116, D08204, doi:10.1029/2010JD015152, 2011a.

Kondo, Y., Sahu, L., Moteki, N., Khan, F., Takegawa, N., Liu, X., Koike, M., and Miyakawa, T.: Consistency and traceability of black carbon measurements made by laser-induced incandescence, thermal-optical transmittance, and filter-based photo-absorption techniques, Aerosol Sci. Tech., 45, 295–312, doi:10.1080/02786826.2010.533215, 2011b.

Kübbeler, M., Hildebrandt, M., Meyer, J., Schiller, C., Hamburger, Th., Jurkat, T., Minikin, A., Petzold, A., Rautenhaus, M., Schlager, H., Schumann, U., Voigt, C., Spichtinger, P., Gayet, J.-F., Gourbeyre, C., and Krämer, M.: Thin and subvisible cirrus and contrails in a subsaturated environment, Atmos. Chem. Phys., 11, 5853–5865, doi:10.5194/acp-11-5853-2011, 2011.

Laborde, M., Mertes, P., Zieger, P., Dommen, J., Baltensperger, U., and Gysel, M.: Sensitivity of the Single Particle Soot Photometer to different black carbon types, Atmos. Meas. Tech., 5, 1031–1043, doi:10.5194/amt-5-1031-2012, 2012a.

Laborde, M., Schnaiter, M., Linke, C., Saathoff, H., Naumann, K.-H., Möhler, O., Berlenz, S., Wagner, U., Taylor, J. W., Liu, D., Flynn, M., Allan, J. D., Coe, H., Heimerl, K., Dahlkötter, F., Weinzierl, B., Wollny, A. G., Zanatta, M., Cozic, J., Laj, P., Hitzenberger, R., Schwarz, J. P.,

ACPD
13, 28751–28818, 2013

and Gysel, M.: Single Particle Soot Photometer intercomparison at the AIDA chamber, Atmos. Meas. Tech., 5, 3077–3097, doi:10.5194/amt-5-3077-2012, 2012b.
Laborde, M., Crippa, M., Tritscher, T., Jurányi, Z., Decarlo, P. F., Temime-Roussel, B., Marchand, N., Eckhardt, S., Stohl, A., Baltensperger, U., Prévôt, A. S. H., Weingartner, E., and Gysel, M.: Black carbon physical properties and mixing state in the European megacity Paris, Atmos. Chem. Phys., 13, 5831–5856, doi:10.5194/acp-13-5831-2013, 2013.
Lee, D. S., Pitari, G., Grewe, V., Gierens, K., Penner, J. E., Petzold, A., Prather, M. J., Schumann, U., Bais, A., Berntsen, T., Iachetti, D., Lim, L. L., and Sausen, R.: Transport impacts on atmosphere and climate: aviation, Atmos. Environ., 44, 4678–4734, doi:10.1016/j.atmosenv.2009.06.005, 2010.
Liu, D., Allan, J., Whitehead, J., Young, D., Flynn, M., Coe, H., McFiggans, G., Fleming, Z. L., and Bandy, B.: Ambient black carbon particle hygroscopic properties controlled by mixing state and composition, Atmos. Chem. Phys., 13, 2015–2029, doi:10.5194/acp-13-2015-2013, 2013.
Liu, L. and Mishchenko, M. I.: Scattering and radiative properties of complex soot and soot-containing aggregate particles, J. Quant. Spectrosc. Ra., 106, 262–273, doi:10.1016/j.jqsrt.2007.01.020, 2007.
Mattis, I., Mueller, D., Ansmann, A., Wandinger, U., Preissler, J., Seifert, P., and Tesche, M.: Ten years of multiwavelength Raman lidar observations of free-tropospheric aerosol layers over central Europe: geometrical properties and annual cycle, J. Geophys. Res.-Atmos., 113, D20202, doi:10.1029/2007JD009636, 2008.
McMeeking, G. R.: The optical, chemical, and physical properties of aerosols and gases emitted by the laboratory combustion of wildland fuels, Ph.D. thesis, Department of Atmospheric Sciences, Colorado State University, 321 pp., 2008.
McMeeking, G. R., Hamburger, T., Liu, D., Flynn, M., Morgan, W. T., Northway, M., Highwood, E. J., Krejci, R., Allan, J. D., Minikin, A., and Coe, H.: Black carbon measurements in the boundary layer over western and northern Europe, Atmos. Chem. Phys., 10, 9393–9414, doi:10.5194/acp-10-9393-2010, 2010.
McMeeking, G. R., Good, N., Petters, M. D., McFiggans, G., and Coe, H.: Influences on the fraction of hydrophobic and hydrophilic black carbon in the atmosphere, Atmos. Chem. Phys., 11, 5099–5112, doi:10.5194/acp-11-5099-2011, 2011.
Metcalf, A. R., Craven, J. S., Ensberg, J. J., Brioude, J., Angevine, W., Sorooshian, A., Duong, H. T., Jonsson, H. H., Flagan, R. C., and Seinfeld, J. H.: Black carbon aerosol

ACPD
13, 28751–28818, 2013

over the Los Angeles Basin during CalNex, J. Geophys. Res.-Atmos., 117, D00V13, doi:10.1029/2011JD017255, 2012.
Mishchenko, M. I., Liu, L., Travis, L. D., and Lacis, A. A.: Scattering and radiative properties of semi-external versus external mixtures of different aerosol types, J. Quant. Spectrosc. Ra., 88, 139–147, doi:10.1016/j.jqsrt.2003.12.032, 2004.
Moosmüller, H., Chakrabarty, R. K., and Arnott, W. P.: Aerosol light absorption and its measurement: a review, J. Quant. Spectrosc. Ra., 110, 844–878, doi:10.1016/j.jqsrt.2009.02.035, 2009.
Moteki, N. and Kondo, Y.: Effects of mixing state on black carbon measurements by laser-induced incandescence, Aerosol Sci. Tech., 41, 398–417, doi:10.1080/02786820701199728, 2007.
Moteki, N. and Kondo, Y.: Dependence of laser-induced incandescence on physical properties of black carbon aerosols: measurements and theoretical interpretation, Aerosol Sci. Tech., 44, 663–675, doi:10.1080/02786826.2010.484450, 2010.
Moteki, N., Kondo, Y., and Nakamura, S.: Method to measure refractive indices of small nonspherical particles: application to black carbon particles, J. Aerosol Sci., 41, 513–521, doi:10.1016/j.jaerosci.2010.02.013, 2010.
Moteki, N., Kondo, Y., Oshima, N., Takegawa, N., Koike, M., Kita, K., Matsui, H., and Kajino, M.: Size dependence of wet removal of black carbon aerosols during transport from the boundary layer to the free troposphere, Geophys. Res. Lett., 39, L13802, doi:10.1029/2012GL052034, 2012.
Müller, D., Ansmann, A., Mattis, I., Tesche, M., Wandinger, U., Althausen, D., and Pisani, G.: Aerosol-type-dependent lidar ratios observed with Raman lidar, J. Geophys. Res.-Atmos., 112, D16202, doi:10.1029/2006JD008292, 2007.
Onasch, T. B., Trimborn, A., Fortner, E. C., Jayne, J. T., Kok, G. L., Williams, L. R., Davidovits, P., and Worsnop, D. R.: Soot particle aerosol mass spectrometer: development, validation, and initial application, Aerosol Sci. Tech., 46, 804–817, doi:10.1080/02786826.2012.663948, 2012.
Oshima, N., Kondo, Y., Moteki, N., Takegawa, N., Koike, M., Kita, K., Matsui, H., Kajino, M., Nakamura, H., Jung, J. S., and Kim, Y. J.: Wet removal of black carbon in Asian outflow: aerosol radiative forcing in East Asia (A-FORCE) aircraft campaign, J. Geophys. Res.-Atmos., 117, D03204, doi:10.1029/2011JD016552, 2012.

ACPD
13, 28751–28818, 2013

Petzold, A., Weinzierl, B., Huntrieser, H., Stohl, A., Real, E., Cozic, J., Fiebig, M., Hendricks, J., Lauer, A., Law, K., Roiger, A., Schlager, H., and Weingartner, E.: Perturbation of the European free troposphere aerosol by North American forest fire plumes during the ICARTT-ITOP experiment in summer 2004, Atmos. Chem. Phys., 7, 5105–5127, doi:10.5194/acp-7-5105-2007, 2007.

Petzold, A., Veira, A., Mund, S., Esselborn, M., Kiemle, C., Weinzierl, B., Hamburger, T., Ehret, G., Lieke, K., and Kandler, K.: Mixing of mineral dust with urban pollution aerosol over Dakar (Senegal): impact on dust physico-chemical and radiative properties, Tellus B, 63, 619–634, doi:10.1111/j.1600-0889.2011.00547.x, 2011.

Petzold, A., Ogren, J. A., Fiebig, M., Laj, P., Li, S.-M., Baltensperger, U., Holzer-Popp, T., Kinne, S., Pappalardo, G., Sugimoto, N., Wehrli, C., Wiedensohler, A., and Zhang, X.-Y.: Recommendations for reporting "black carbon" measurements, Atmos. Chem. Phys., 13, 8365–8379, doi:10.5194/acp-13-8365-2013, 2013.

Posfai, M., Simonics, R., Li, J., Hobbs, P. V., and Buseck, P. R.: Individual aerosol particles from biomass burning in southern Africa: 1. Compositions and size distributions of carbonaceous particles, J. Geophys. Res.-Atmos., 108, 8483, doi:10.1029/2002JD002291, 2003.

Posfai, M., Gelencser, A., Simonics, R., Arato, K., Li, J., Hobbs, P. V., and Buseck, P. R.: Atmospheric tar balls: particles from biomass and biofuel burning, J. Geophys. Res.-Atmos., 109, D06213, doi:10.1029/2003JD004169, 2004.

Pratt, K. A., Murphy, S. M., Subramanian, R., DeMott, P. J., Kok, G. L., Campos, T., Rogers, D. C., Prenni, A. J., Heymsfield, A. J., Seinfeld, J. H., and Prather, K. A.: Flight-based chemical characterization of biomass burning aerosols within two prescribed burn smoke plumes, Atmos. Chem. Phys., 11, 12549–12565, doi:10.5194/acp-11-12549-2011, 2011.

Quennehen, B., Schwarzenboeck, A., Schmale, J., Schneider, J., Sodemann, H., Stohl, A., Ancellet, G., Crumeyrolle, S., and Law, K. S.: Physical and chemical properties of pollution aerosol particles transported from North America to Greenland as measured during the POLARCAT summer campaign, Atmos. Chem. Phys., 11, 10947–10963, doi:10.5194/acp-11-10947-2011, 2011.

Quennehen, B., Schwarzenboeck, A., Matsuki, A., Burkhart, J. F., Stohl, A., Ancellet, G., and Law, K. S.: Anthropogenic and forest fire pollution aerosol transported to the Arctic: observations from the POLARCAT-France spring campaign, Atmos. Chem. Phys., 12, 6437–6454, doi:10.5194/acp-12-6437-2012, 2012.

ACPD
13, 28751–28818, 2013

Ramanathan, V. and Carmichael, G.: Global and regional climate changes due to black carbon, Nat. Geosci., 1, 221–227, doi:10.1038/ngeo156, 2008.
Ramanathan, V. and Feng, Y.: Air pollution, greenhouse gases and climate change: global and regional perspectives, Atmos. Environ., 43, 37–50, doi:10.1016/j.atmosenv.2008.09.063, 2009.
Real, E., Law, K. S., Weinzierl, B., Fiebig, M., Petzold, A., Wild, O., Methven, J., Arnold, S., Stohl, A., Huntrieser, H., Roiger, A., Schlager, H., Stewart, D., Avery, M., Sachse, G., Browell, E., Ferrare, R., and Blake, D.: Processes influencing ozone levels in Alaskan forest fire plumes during long-range transport over the North Atlantic, J. Geophys. Res.-Atmos., 112, D10S41, doi:10.1029/2006JD007576, 2007.
Rocadenbosch, F., Md Reba, M. N., Sicard, M., and Comerón, A.: Practical analytical backscatter error bars for elastic one-component lidar inversion algorithm, Appl. Optics, 49, 3380–3393, doi:10.1364/AO.49.003380, 2010.
Sahu, L. K., Kondo, Y., Moteki, N., Takegawa, N., Zhao, Y., Cubison, M. J., Jimenez, J. L., Vay, S., Diskin, G. S., Wisthaler, A., Mikoviny, T., Huey, L. G., Weinheimer, A. J., and Knapp, D. J.: Emission characteristics of black carbon in anthropogenic and biomass burning plumes over California during ARCTAS-CARB 2008, J. Geophys. Res.-Atmos., D16302, 117, doi:10.1029/2011JD017401, 2012.
Scarnato, B. V., Vahidinia, S., Richard, D. T., and Kirchstetter, T. W.: Effects of internal mixing and aggregate morphology on optical properties of black carbon using a discrete dipole approximation model, Atmos. Chem. Phys., 13, 5089–5101, doi:10.5194/acp-13-5089-2013, 2013.
Schmale, J., Schneider, J., Jurkat, T., Voigt, C., Kalesse, H., Rautenhaus, M., Lichtenstern, M., Schlager, H., Ancellet, G., Arnold, F., Gerding, M., Mattis, I., Wendisch, M., and Borrmann, S.: Aerosol layers from the 2008 eruptions of Mount Okmok and Mount Kasatochi: in situ upper troposphere and lower stratosphere measurements of sulfate and organics over Europe, J. Geophys. Res.-Atmos., 115, D00L07, doi:10.1029/2009JD013628, 2010.
Schumann, U., Mayer, B., Gierens, K., Unterstrasser, S., Jessberger, P., Petzold, A., Voigt, C., and Gayet, J. F.: Effective radius of ice particles in cirrus and contrails, J. Atmos. Sci., 68, 300–321, doi:10.1175/2010jas3562.1, 2011.
Schumann, U., Jeßberger, P., and Voigt, C.: Contrail ice particles in aircraft wakes and their climatic importance, Geophys. Res. Lett., 40, 2867–2872, doi:10.1002/grl.50539, 2013.

ACPD
13, 28751–28818, 2013

Schwarz, J. P., Gao, R. S., Fahey, D. W., Thomson, D. S., Watts, L. A., Wilson, J. C., Reeves, J. M., Darbeheshti, M., Baumgardner, D. G., Kok, G. L., Chung, S. H., Schulz, M., Hendricks, J., Lauer, A., Karcher, B., Slowik, J. G., Rosenlof, K. H., Thompson, T. L., Langford, A. O., Loewenstein, M., and Aikin, K. C.: Single-particle measurements of midlatitude black carbon and light-scattering aerosols from the boundary layer to the lower stratosphere, J. Geophys. Res.-Atmos., 111, D16207, doi:10.1029/2006JD007076, 2006.

Schwarz, J. P., Gao, R. S., Spackman, J. R., Watts, L. A., Thomson, D. S., Fahey, D. W., Ryerson, T. B., Peischl, J., Holloway, J. S., Trainer, M., Frost, G. J., Baynard, T., Lack, D. A., de Gouw, J. A., Warneke, C., and Del Negro, L. A.: Measurement of the mixing state, mass, and optical size of individual black carbon particles in urban and biomass burning emissions, Geophys. Res. Lett., 35, L13810, doi:10.1029/2008gl033968, 2008a.

Schwarz, J. P., Spackman, J. R., Fahey, D. W., Gao, R. S., Lohmann, U., Stier, P., Watts, L. A., Thomson, D. S., Lack, D. A., Pfister, L., Mahoney, M. J., Baumgardner, D., Wilson, J. C., and Reeves, J. M.: Coatings and their enhancement of black carbon light absorption in the tropical atmosphere, J. Geophys. Res.-Atmos., 113, D03203, doi:10.1029/2007jd009042, 2008b.

Schwarz, J. P., Spackman, J. R., Gao, R. S., Watts, L. A., Stier, P., Schulz, M., Davis, S. M., Wofsy, S. C., and Fahey, D. W.: Global-scale black carbon profiles observed in the remote atmosphere and compared to models, Geophys. Res. Lett., 37, L23804, doi:10.1029/2010gl046007, 2010.

Sedlacek III, A. J., Lewis, E. R., Kleinman, L., Xu, J., and Zhang, Q.: Determination of and evidence for non-core-shell structure of particles containing black carbon using the Single-Particle Soot Photometer (SP2), Geophys. Res. Lett., 39, L06802, doi:10.1029/2012GL050905, 2012.

Shiraiwa, M., Kondo, Y., Iwamoto, T., and Kita, K.: Amplification of light absorption of black carbon by organic coating, Aerosol Sci. Tech., 44, 46–54, doi:10.1080/02786820903357686, 2010.

Stephens, M., Turner, N., and Sandberg, J.: Particle identification by laser-induced incandescence in a solid-state laser cavity, Appl. Optics, 42, 3726–3736, doi:10.1364/AO.42.003726, 2003.

Tesche, M., Ansmann, A., Mueller, D., Althausen, D., Engelmann, R., Freudenthaler, V., and Gross, S.: Vertically resolved separation of dust and smoke over Cape Verde using multiwavelength Raman and polarization lidars during Saharan Mineral Dust Experiment 2008, J. Geophys. Res.-Atmos., 114, D13202, doi:10.1029/2009JD011862, 2009.

ACPD
13, 28751–28818, 2013

Tesche, M., Mueller, D., Gross, S., Ansmann, A., Althausen, D., Freudenthaler, V., Weinzierl, B., Veira, A., and Petzold, A.: Optical and microphysical properties of smoke over Cape Verde inferred from multiwavelength lidar measurements, Tellus B, 63, 677–694, doi:10.1111/j.1600-0889.2011.00549.x, 2011.

Voigt, C., Schumann, U., Jurkat, T., Schäuble, D., Schlager, H., Petzold, A., Gayet, J.-F., Krämer, M., Schneider, J., Borrmann, S., Schmale, J., Jessberger, P., Hamburger, T., Lichtenstern, M., Scheibe, M., Gourbeyre, C., Meyer, J., Kübbeler, M., Frey, W., Kalesse, H., Butler, T., Lawrence, M. G., Holzäpfel, F., Arnold, F., Wendisch, M., Döpelheuer, A., Gottschaldt, K., Baumann, R., Zöger, M., Sölch, I., Rautenhaus, M., and Dörnbrack, A.: In-situ observations of young contrails – overview and selected results from the CONCERT campaign, Atmos. Chem. Phys., 10, 9039–9056, doi:10.5194/acp-10-9039-2010, 2010.

Voigt, C., Schumann, U., Jessberger, P., Jurkat, T., Petzold, A., Gayet, J. F., Kraemer, M., Thornberry, T., and Fahey, D. W.: Extinction and optical depth of contrails, Geophys. Res. Lett., 38, L11806, doi:10.1029/2011GL047189, 2011.

Weinzierl, B., Petzold, A., Esselborn, M., Wirth, M., Rasp, K., Kandler, K., Schuetz, L., Koepke, P., and Fiebig, M.: Airborne measurements of dust layer properties, particle size distribution and mixing state of Saharan dust during SAMUM 2006, Tellus B, 61, 96–117, doi:10.1111/j.1600-0889.2008.00392.x, 2009.

Weinzierl, B., Sauer, D., Esselborn, M., Petzold, A., Veira, A., Rose, M., Mund, S., Wirth, M., Ansmann, A., Tesche, M., Gross, S., and Freudenthaler, V.: Microphysical and optical properties of dust and tropical biomass burning aerosol layers in the Cape Verde region-an overview of the airborne in situ and lidar measurements during SAMUM-2, Tellus B, 63, 589–618, doi:10.1111/j.1600-0889.2011.00566.x, 2011.

Weinzierl, B., Sauer, D., Minikin, A., Reitebuch, O., Dahlkoetter, F., Mayer, B., Emde, C., Tegen, I., Gasteiger, J., Petzold, A., Veira, A., Kueppers, U., and Schumann, U.: On the visibility of airborne volcanic ash and mineral dust from the pilot's perspective in flight, Phys. Chem. Earth, 45–46, 87–102, doi:10.1016/j.pce.2012.04.003, 2012.

Wendisch, M., Coe, H., Baumgardner, D., Brenguier, J.-L., Dreiling, V., Fiebig, M., Formenti, P., Hermann, M., Krämer, M., Levin, Z., Maser, R., Mathieu, E., Nacass, P., Noone, K., Osborne, S., Schneider, J., Schütz, L., Schwarzenböck, A., Stratmann, F., and Wilson, J. C.: Aircraft particle inlets: state-of-the-art and future needs, B. Am. Meteotol. Soc., 85, 89–91, doi:10.1175/BAMS-85-1-89, 2004.

ACPD
13, 28751–28818, 2013

Wiedinmyer, C., Akagi, S. K., Yokelson, R. J., Emmons, L. K., Al-Saadi, J. A., Orlando, J. J., and Soja, A. J.: The Fire INventory from NCAR (FINN): a high resolution global model to estimate the emissions from open burning, Geosci. Model Dev., 4, 625–641, doi:10.5194/gmd-4-625-2011, 2011.

ACPD
13, 28751–28818, 2013

Table 1. Size ranges of the aerosol instrumentation onboard the Falcon aircraft considered in this study during the flights on 16 September 2011. The first column displays the name of the instrument, the second column the measured property, and the third column the respective size range. CPC, Condensation Particle Counter; CPSA, Condensation Particle Size Analyser; SP2, Single Particle Soot Photometer; LSD, light scattering detector; BID, broadband incandescence detector; NID, narrowband incandescence detector; PSD, position sensitive detector; FSSP-300, Forward Scattering Spectrometer Probe.

Instrument	Property	Size range
CPC/CPSA	integral number concentration[a] of ultrafine particles	$0.004 < D_{opt} < D_{cutoff}$ µm
SP2	LSD	
	single particle optical diameter of rBC-free particles	$0.14 < D_{opt} < 0.29$ µm
	ambient number size distribution of rBC-free particles	$0.14 < D_{opt} < 0.29$ µm
	BID, NID	
	single particle rBC mass	$0.5 < m_{rBC} < 80.3$ fg
	ambient rBC mass size distribution	$0.08 < D_{rBC} < 0.44$ µm
	LSD, BID, NID, PSD	
	Leading-edge-only (LEO) fit:	
	single particle optical diameter of rBC-free and rBC-containing particles	$\sim 0.15 < D_{opt} <\sim 0.55$ µm (cut-offs dependent on rBC fraction)
	coating thickness of rBC-containing particles	(see Sect. 5.4)
FSSP-300	ambient size distribution[b]	nominal size range $0.3 < D_{opt} < 30$ µm
Falcon standard instrumentation	T, p, RH, 3-D-wind velocity	

[a] Aerosol in-situ instruments operated inside the cabin of the Falcon behind an isokinetic inlet. The inlet system has an upper cut-off diameter D_{cutoff} where 50 % of the particles are carried into the isokinetic inlet, depending on air speed and outside pressure. For typical Falcon speed, the cut-off decreases from roughly 2.5 µm at ground level to roughly 1.5 µm at 10 km altitude (Fiebig, 2001; Wendisch et al., 2004).

[b] Aerosol in-situ instruments sampling at wing stations.

ACPD
13, 28751–28818, 2013

Table 2. List of research flights during CONCERT 2011. For each flight the lower and upper boundary[a] of the detected aerosol layers is given. The Pagami Creek fire plume is written in bold type. OP, Oberpfaffenhofen; NB, Neubrandenburg-Trollenhagen; TRA, Temporary Restricted Area.

Flight ID	Route	Take-off time UTC/hh:mm	Landing time UTC/hh:mm	Presence of Elevated Layers	
				Lower boundary km^{-1}	Upper boundary km^{-1}
#110907a	OP – Leipzig – OP	06:21	07:53		
				2.6	3.0
				3.7	5.3
				3.4	3.9
				2.0	3.2
				10.1	10.7
#110916a	OP – Mecklenburg – NB	10:48	13:20		
				1.8	2.0
				2.2	3.4
				3.4	4.5
				10.1	**11.6**
#110916b	NB – Leipzig – OP	14:54	17:48		
				2.0	3.3
				8.7	**9.5**
				10.9	**11.3**
#110917a	OP – Hamburg – Brandenburg – OP	11:05	13:54		
				2.2	3.0
				3.0	4.3
				4.6	5.7
				2.1	3.6
#110922a	OP – Frankfurt – Bergen	07:03	09:18		
				4.7	5.4
#110922b	Bergen – OP	10:20	13:20		
				6.5	6.9
#110924a	OP – TRA Weser – OP	09:44	13:12		
				1.7	2.7
				3.1	4.6
				1.8	4.9
#110927a	OP – TRA Weser – OP	06:57	10:27		
				1.5	2.7
				2.7	4.6
#110929a	OP – Catania	08:52	12:19		
				3.3	3.3
#110930a	Catania – Stromboli – Etna – Catania	06:34	09:34		
				0.4	2.2
				0.9	0.9
				3.5	3.5
				3.0	3.0
#110930b	Catania – OP	10:55	14:45		
				2.0	3.3

[a] The boundaries are derived from the in-situ measurements, representing the minimal vertical depth of the layers.

ACPD
13, 28751–28818, 2013

Table 3. rBC characteristics and characteristics of the total particle number size distributions in the Pagami Creek smoke plume. Shown are the minimum, median, and maximum values of rBC mass concentrations, the parameters of the log-normal fit to the rBC mass size distribution, the parameters of the log-normal fit to the total number size distribution, and stp-ambient conversion factors of 14 sequences during the forest fire aerosol layer measurements. Values in italics are extrapolated from total number concentration values. In comparison to the rBC mass concentration in the Pagami Creek fire within the SP2 size range (0.03–0.29 $\mu g\,m^{-3}$) the free tropospheric background sequence has a mean rBC mass concentration of $< 0.004\,\mu g\,m^{-3}$. GSD, geometric standard deviation; CMD, count median diameter.

Parameter		Sequence with rBC mass concentration minimum	median	maximum
rBC mass concentration (in SP2 size range) (stp)				
	$\mu g\,m^{-3}$	0.03	0.12	0.29
Parameters of log-normal fit to rBC mass size distribution as function of D_{rBC}(stp)				
rBC total mass concentration	$\mu g\,m^{-3}$	0.03	0.16	0.35
GSD	–	1.75	1.70	1.70
CMD	nm	121	144	150
Parameters of log-normal fit to total particle number size distribution as a function of D_{opt}(stp)				
N_1	cm^{-3}	1077	1517	760
GSD_1	–	1.36	1.30	1.30
CMD_1	nm	70	70	70
N_2	cm^{-3}	130	641	957
GSD_2	–	1.46	1.41	1.44
CMD_2	nm	243	251	281
N_3	cm^{-3}	1	–	–
GSD_3	–	1.10	–	–
CMD_3	nm	550	–	–
stp factor	–	3.92	3.93	4.15

ACPD
13, 28751–28818, 2013

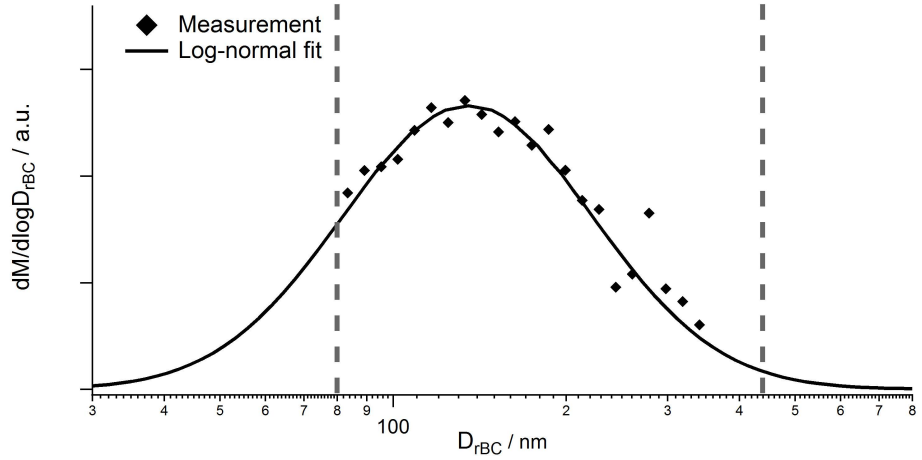

Fig. 1. Scheme illustrating the determination of rBC mass size distributions from SP2 measurements (diamonds), the measurement range (between grey dashed lines), and log-normal fit (black line). Based on the fit, the total rBC mass concentration can be derived. For details see Sect. 2.2. dM/dlogD_{rBC}: normalized mass concentrations (in arbitrary units; a.u.).

ACPD
13, 28751–28818, 2013

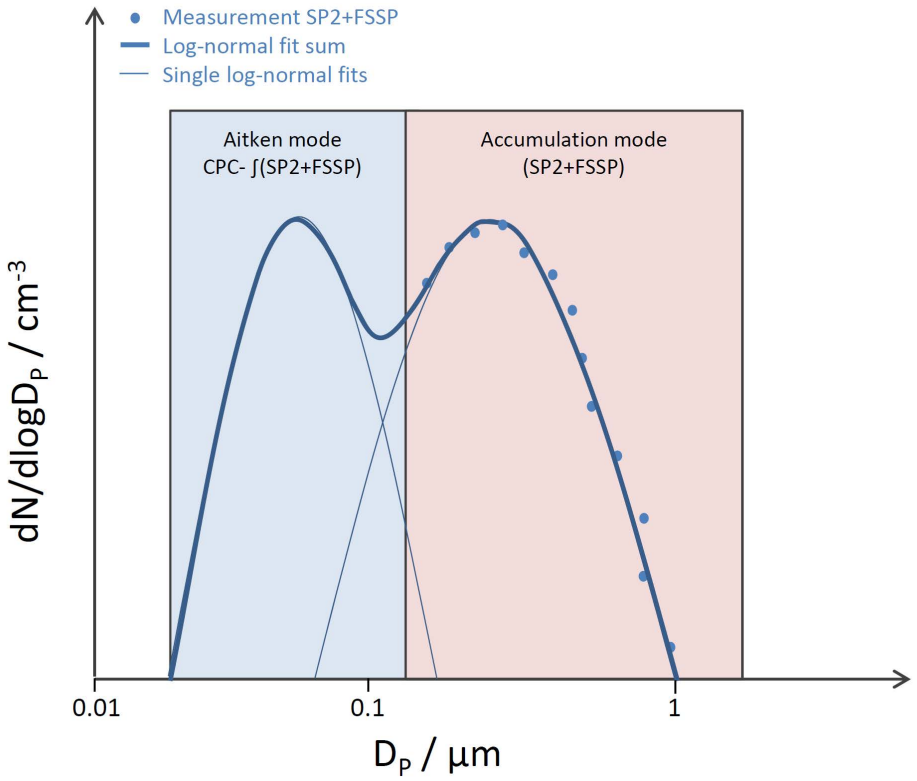

Fig. 2. Scheme of the determination of number size distributions: dots represent the combined measurements of SP2 and FSSP-300 (accumulation mode; red box). The integral number concentration of particles smaller 0.14 µm (Aitken mode; blue box) is derived from the difference of the CPC number concentration to integral number concentration of SP2 and FSSP-300 in the accumulation mode. Log-normal fits are applied to the measured size distribution and extrapolated toward smaller sizes. For details see Sect. 2.2.

ACPD
13, 28751–28818, 2013

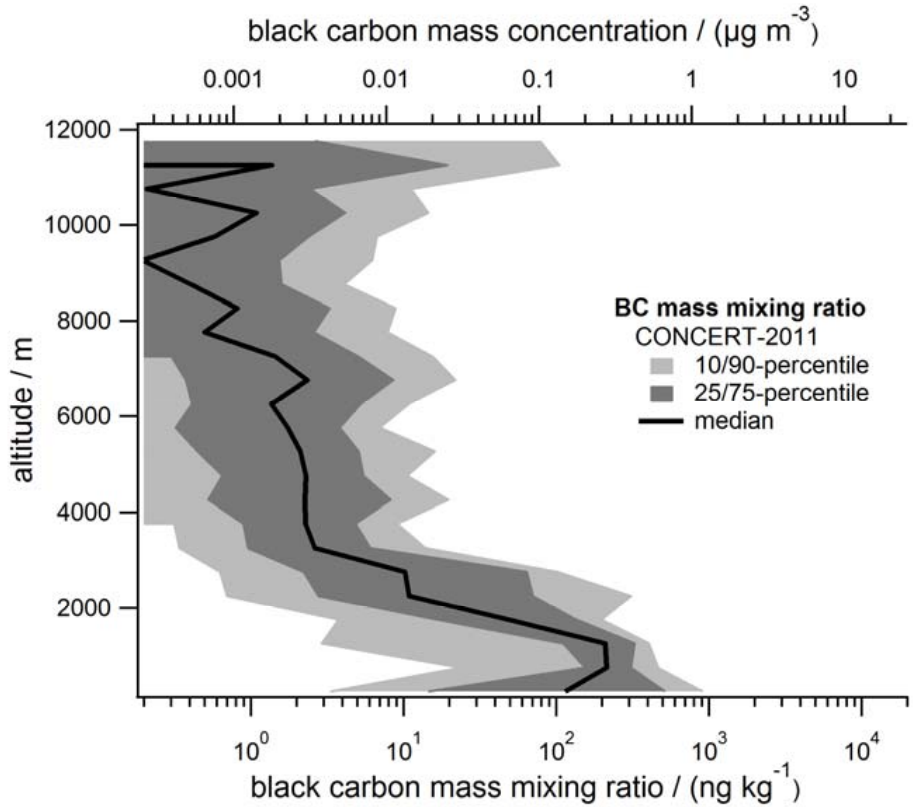

Fig. 3. Vertical profile (stp) of the rBC mass mixing ratio (MMR) and rBC mass concentration (m) for all flights during CONCERT 2011 measured with the SP2 as median (black), 25-/75-percentile (dark grey), and 10-/90-percentile (light grey) for 500 m vertical intervals and a temporal resolution of 10 s. Values are valid for the approximate size range of 80–440 nm. The mass mixing ratio MMR was calculated from the mass concentration m (MMR [ng kg^{-1}] = m [ng m^{-3}]/1.29 [kg m^{-3}]).

ACPD
13, 28751–28818, 2013

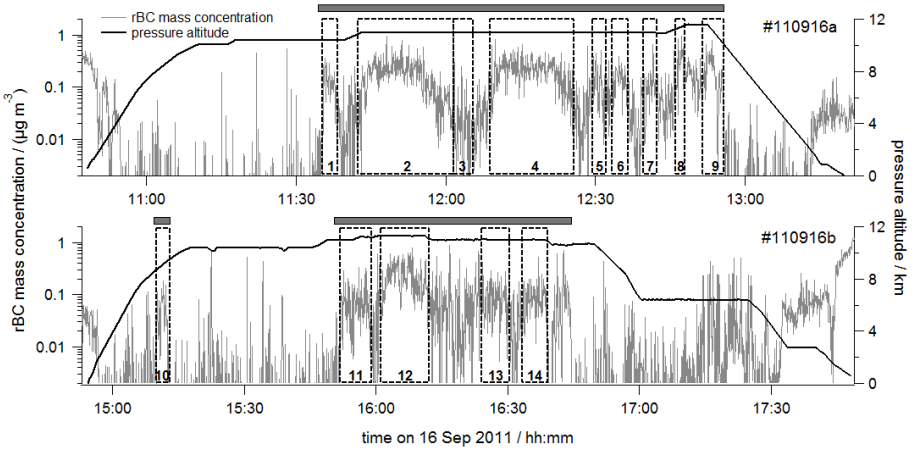

Fig. 4. Time series of the rBC mass concentration (stp) in the SP2 size range (grey lines) for flight #110916a (up) and flight #110916b (bottom). The flight altitude is shown in black lines. The grey bars represent the sequences of continuous forest fire aerosol layer sampling, i.e. the flight time in the area where the aerosol layer was situated. The dashed boxes represent sequences, which are used for detailed analysis. These 14 sequences were chosen to represent part of the aerosol layer with high loads as well with low loads without interference of other aerosol sources such as aircraft emissions.

ACPD
13, 28751–28818, 2013

Fig. 5. Photograph of the Pagami Creek plume taken from DLR Falcon research aircraft over Germany (16 September 2011 12:11 UTC; 11.1 km a.s.l.).

ACPD
13, 28751–28818, 2013

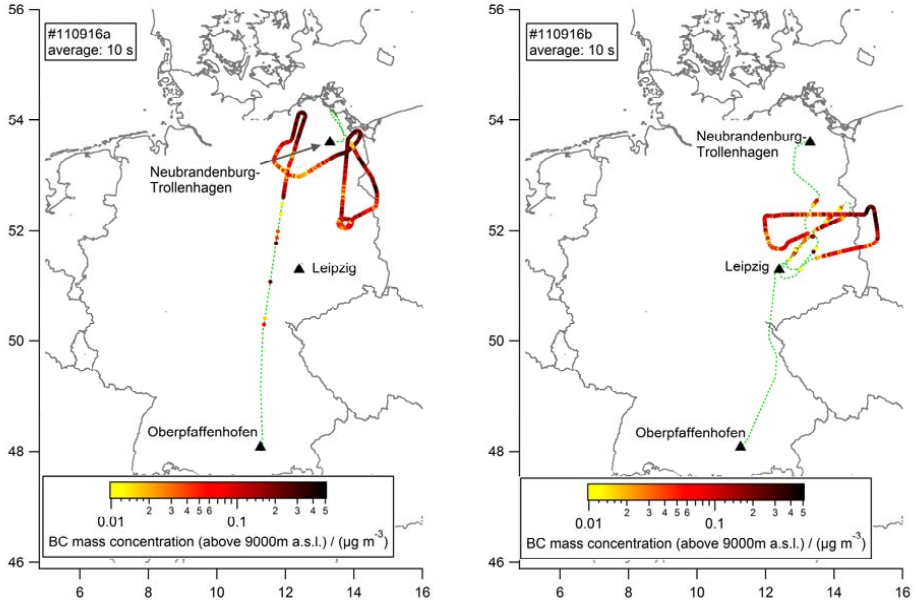

Fig. 6. Flight tracks for flight #110916a (left) and #110916b (right) on 16 September 2011 with averaged (10 s) rBC mass concentrations (stp) color-coded along the flight track. For clarity, only data for altitudes larger 9 km a.s.l. are shown and rBC mass concentrations < 0.01 µg m^{-3} were skipped.

ACPD
13, 28751–28818, 2013

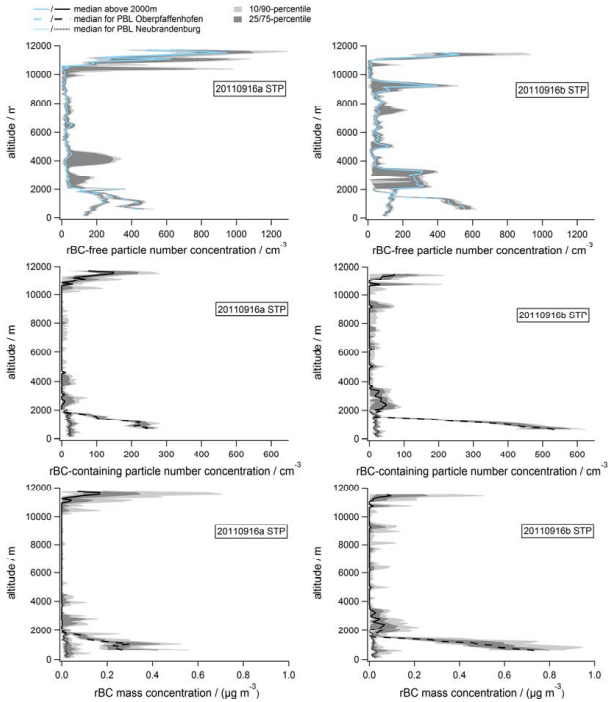

Fig. 7. Vertical profiles (stp) of flight #110916a (left) and #110916b (right) on 16 September 2011 for rBC-free particle number concentration (upper panels), rBC-containing particle number concentration (middle panels), and rBC mass concentration (bottom panels) measured with the SP2 as median (blue and black), 25-/75-percentile (dark grey), and 10-/90-percentile (light grey) for 100 m vertical intervals. Below 2000 m the dataset is split into the PBL of Oberpfaffenhofen (593 m a.s.l.; dashed line) and Neubrandenburg (69 m a.s.l.; dotted line). Values are representative for the approximate size range of 140–290 nm and 80–440 nm for the rBC-free particles (upper panels) and the rBC particles (middle and bottom panels), respectively.

ACPD
13, 28751–28818, 2013

Aerosol and black carbon properties in the Pagami Creek smoke plume

F. Dahlkötter et al.

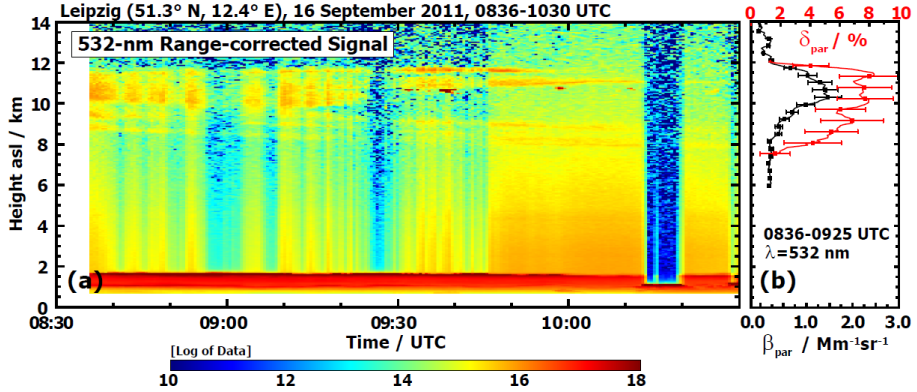

Fig. 8. (a) Time-height cross-section of the 532 nm range-corrected backscatter signal of the lidar system in Leipzig, and **(b)** vertical profiles of particle backscatter coefficient β_{par} (black curve) and particle depolarization ratio δ_{par} with error bars (red curve) for the time interval 08:35–09:30 UTC. The optical thickness (at 532 nm) of the observed aerosol layer is derived to be 0.15–0.20.

ACPD
13, 28751–28818, 2013

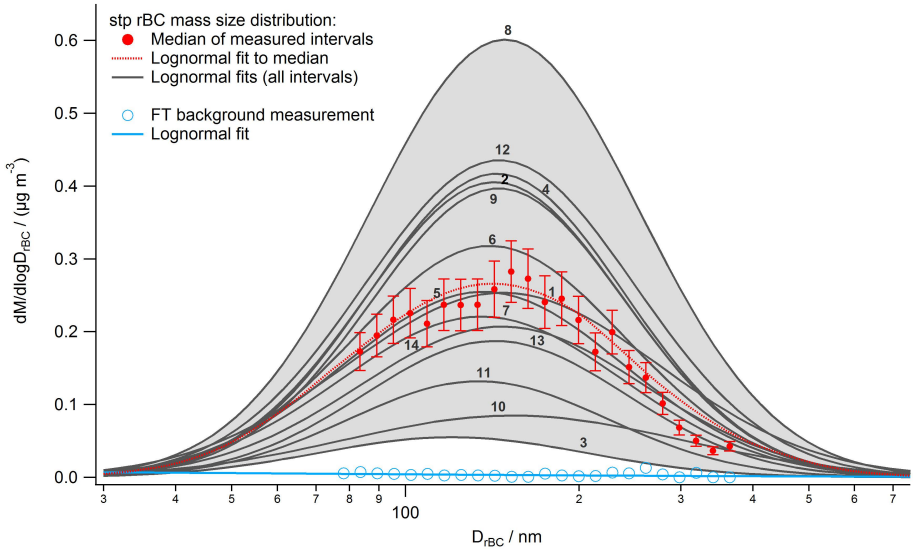

Fig. 9. Median rBC mass size distribution (red dots) out of the 14 measurement sequences (see Fig. 4) in the Pagami Creek plume. Log-normal fits (solid lines) are shown for all sequences for the measured size range of 80–250 nm. The grey shaded area represents the range between maximum and minimum log-normal fit. The mean total rBC mass concentration (with accounting for the data outside the SP2 range) is 0.03–0.35 µg m^{-3} (stp) for the 14 sequences in forest fire layer, indicated by the numbering. Error bars represent 15 % uncertainty (see Sect. 2.2). For comparison the rBC mass of a free tropospheric (FT) background sequence (blue) is shown.

ACPD
13, 28751–28818, 2013

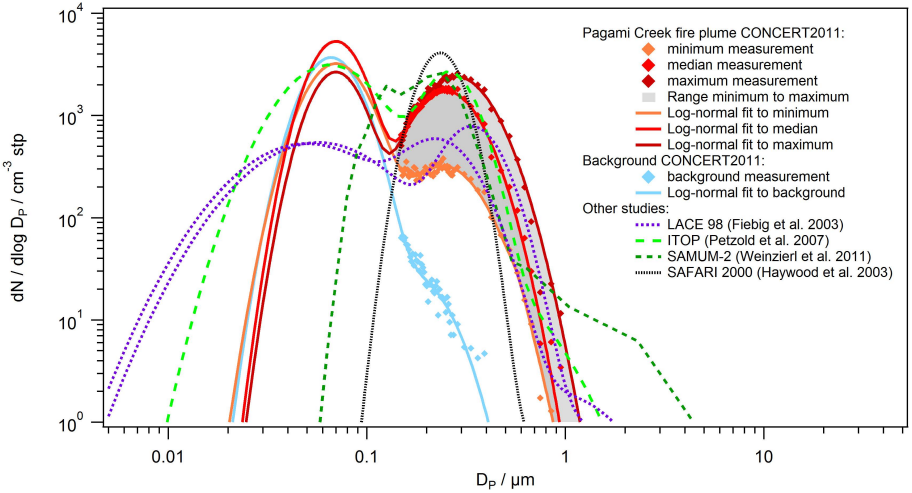

Fig. 10. Number size distributions (stp) for background aerosol (blue markers), minimum (orange markers), median (red markers), maximum (dark red markers), and range (light grey area) of measurements in the Pagami Creek forest fire plume. Number size distributions are extrapolated by log-normal fits for the minimum, median, maximum, and background measurements (orange, red, dark red, and blue solid lines), and compared to forest fire plumes (dashed lines) from LACE 98 (purple) as ambient values, ICARTT-ITOP (light green), SAMUM-2 (dark green), and SAFARI 2000 (black). Normalized values from SAFARI 2000, showing only the accumulation mode due to a lack of measurements for particle sizes < 100 nm, are scaled to similar magnitudes.

ACPD
13, 28751–28818, 2013

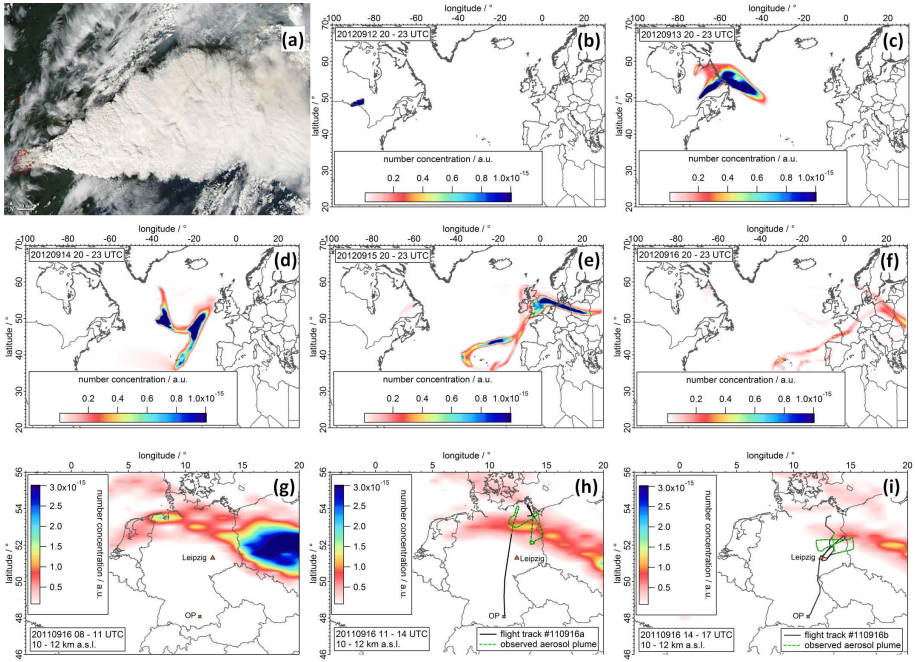

Fig. 11. Evolution and dispersion of the Pagami Creek smoke plume calculated with HYSPLIT. **(a)** MODIS picture of Pagami Creek fire in Minnesota (USA) on 12 September 2011 18:50 UTC (NASA images courtesy Jeff Schmaltz, MODIS Rapid Response Team at NASA GSFC. Caption by Michon Scott.); **(b–f)** daily evolution of the plume vertically integrated from 6–14 km from 12 September 2011 **(b)** through to 16 September 2011 **(f)** for time period 20–23 UTC on each day; **(g–i)** dispersion of the plume over Germany vertically integrated from 10–12 km for the 16 September 2011 08–11 UTC **(g)**, 11–14 UTC **(h)**, and 14–17 UTC **(i)** and locations of Oberpfaffenhofen (OP; star) and Leipzig (triangle). Green dashed lines in **(h)** and **(i)** represent the sequences where the Pagami Creek fire plume was measured.

ACPD
13, 28751–28818, 2013

Aerosol and black carbon properties in the Pagami Creek smoke plume

F. Dahlkötter et al.

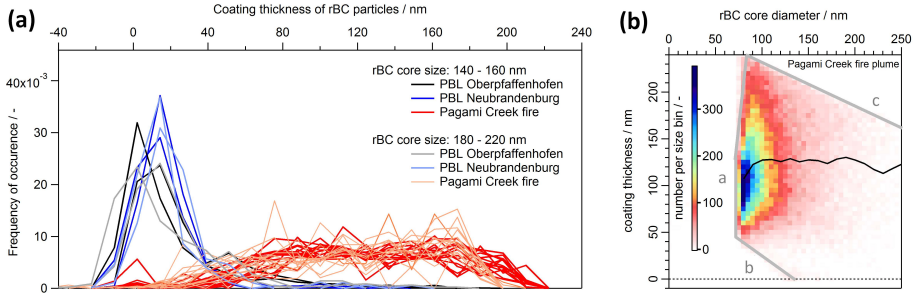

Fig. 12. (a) Histograms of the coating thickness for 14 sequences (see Fig. 4) inside the Pagami Creek forest fire aerosol layer (red) and for fresh boundary layer aerosols in Oberpfaffenhofen, near Munich, and Neubrandenburg in black and blue, respectively, for rBC cores sizes of 140–160 nm (intense color) and 180–220 nm (light color). **(b)** The relationship between rBC core diameter and coating thickness for all 14 sequences in the forest fire aerosol layer is shown as color-coded 2-D histogram including the median coating thickness (black line). The methodological boundaries are indicated by grey lines (a: rBC core below BID lower detection limit; b: scattering signal below LSD lower detection limit; c: scattering signal above LSD higher detection limit).

ACPD
13, 28751–28818, 2013

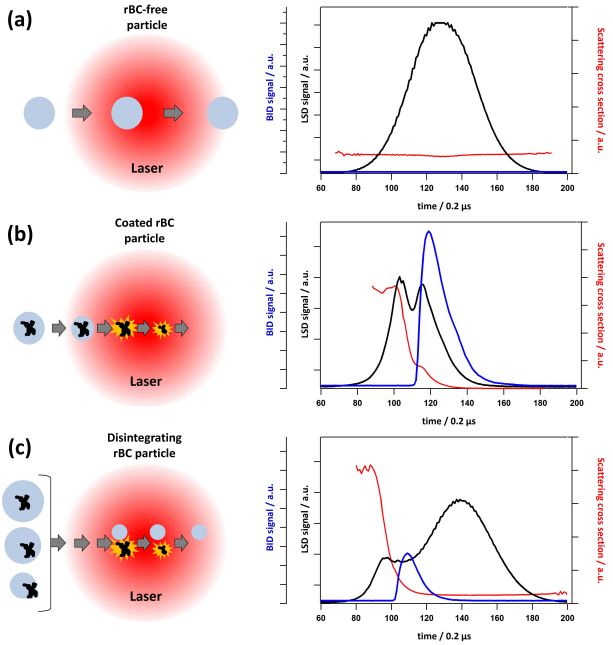

Fig. 13. SP2 raw signals for selective particles with LSD signal (black) and BID signal (blue) and the scattering cross-section (red) for an rBC-free particle **(a)**, a coated rBC particle **(b)**, and a disintegrating rBC particle **(c)**. Schematics for the particle-laser-interaction for each raw signal plot are shown on the left. For the disintegrating rBC particle in **(c)** several initial structures are possible: a very thickly coated rBC particle (up); a thickly coated particle with an eccentrically located rBC core (middle); a rBC particle located at the surface of a rBC-free particle (bottom). For reasons of depiction the size of the schematically shown particles (left) is enlarged compared to the laser diameter. The scattering cross-section was obtained by dividing the scattering signal by the laser intensity profile. The incandescence is indicated by yellow stars.

ACPD
13, 28751–28818, 2013

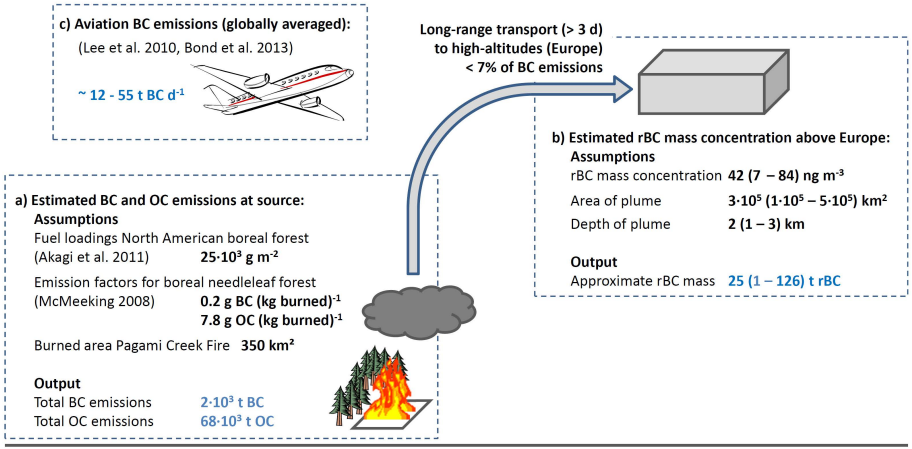

Fig. 14. Schematic for the BC mass import of the Pagami Creek fire: **(a)** calculation of total BC and OC emission from the fire based on fuel loadings, emission factors, and burned area; **(b)** BC mass import to the UTLS region above Europe based on the dispersion of the plume and measured rBC mass concentrations as a best guess (and total range); **(c)** comparison to daily BC emissions of global aviation.

ACPD
13, 28751–28818, 2013